AGU PUBLICATIONS

Geophysical Research Letters

RESEARCH LETTER
10.1002/2014GL060080

Key Points:
- Great and small circle APWP parametrization with paleocolatitude correction
- Paleolongitude can be derived from apparent polar wander path
- Reconstruction of East Gondwana since 140 Ma is reevaluated

Supporting Information:
- Readme
- Text S1–S3, Tables S1 and S2, and Figures S1–S13
- Movie S1
- Movie S2

Correspondence to:
L. Wu,
lwu2@ualberta.ca

Citation:
Wu, L., and V. A. Kravchinsky (2014), Derivation of paleolongitude from the geometric parametrization of apparent polar wander path: Implication for absolute plate motion reconstruction, *Geophys. Res. Lett.*, *41*, doi:10.1002/2014GL060080.

Received 25 APR 2014
Accepted 15 JUN 2014
Accepted article online 18 JUN 2014

Derivation of paleolongitude from the geometric parametrization of apparent polar wander path: Implication for absolute plate motion reconstruction

Lei Wu[1] and Vadim A. Kravchinsky[1]

[1]Department of Physics, University of Alberta, Edmonton, Alberta, Canada

Abstract Obtaining ancient longitude position of continents in the past has always been a challenge for plate tectonic reconstructions. Paleomagnetism has been commonly used to reconstruct paleolatitudes and relative rotations but not paleolongitudes. In this work, we present a synthesized method to derive paleolongitude by geometrically parametrizing apparent polar wander path (APWP). Great and small circle modeling are implemented concurrently to the identified APWP tracks to calculate the paleomagnetic Euler parameters (stage rotation pole and rotation angle). From the Euler parameters of the optimal fitting option, the absolute motion history can be restored for the reference geometries. Using our method as well as the results from relative plate motion studies, we reevaluate the dispersion history of East Gondwana since 140 Ma. To further test the validity of our method, we compare the predictions from four other absolute motion models mainly in paleolatitude movement, longitudinal variation, and great circle distance, which suggest the most similarity with the global hybrid reference frame.

1. Introduction

Quantitatively decoding the absolute motion history of lithospheric plates has been one of the most long-standing challenges since the age of plate tectonics. Motivated by the idea that hot spots are surficial expressions of plumes rising from the lower mantle and that their track geometry might indicate the motion of the lithospheric plates [*Morgan*, 1971], researchers have been striving to establish the hot spots absolute plate motion reference frame for decades [e.g., *Müller et al*., 1993; *O'Neill et al*., 2005; *Torsvik et al*., 2008a; *Doubrovine et al*., 2012]. The constant endeavor to improve the hot spots reference frame is prompted by the unanimous evidence that hot spots are not fixed in the mantle, with the most canonical demonstration of rapid southward motion of the Hawaiian hot spot during Late Cretaceous to Paleogene [*Tarduno*, 2007]. Through the modeling of plume motions, recent hot spot reference frames seem to provide more compatible reconstructions with geologic and geophysical observations during 0–130 Ma [e.g., *Doubrovine et al*., 2012]. For reconstructions earlier than 130 Ma, however, workers still have to rely on paleomagnetic data despite the endless complaints about its incapability in providing paleolongitude.

In quest of the solution to the absolute plate motion reconstruction beyond the hot spot frame, there are several notable attempts in recent years. Using the global hybrid reference frame, *Torsvik et al*. [2008b] proposed an absolute plate reconstruction model by correlating large igneous provinces and deep mantle heterogeneities at the core-mantle boundary. However, this model was built on the assumption of zero longitudinal motion of Africa before 100 Ma which still needs justification. *van der Meer et al*. [2010] established a sinking slab remnant reference frame by linking lower mantle slab remnants with the global orogenic belts reconstructions. They assumed a vertical slab sinking at an average rate of 12 ± 3 mm/yr and the resulting reconstruction bore up to 18° westward discrepancies with the coeval plate reconstructions from the hybrid reference frame [*Torsvik et al*., 2008a]. Recently, *Mitchell et al*. [2012] presented a true polar wander (TPW) derived reference frame by tracing the moving trajectory of supercontinents centers in the deep geologic history. This reference frame was established from the paleomagnetic data of *Torsvik et al*. [2008a] for the reconstruction during 0–260 Ma where they assumed the stable geoid highs. We note, however, all these reference frames widely used by the community were constructed under extra assumptions which are still open to debate. Alternative methods, which are independent of those assumptions, are in great demand for any geodynamic study involving absolute plate kinematics.

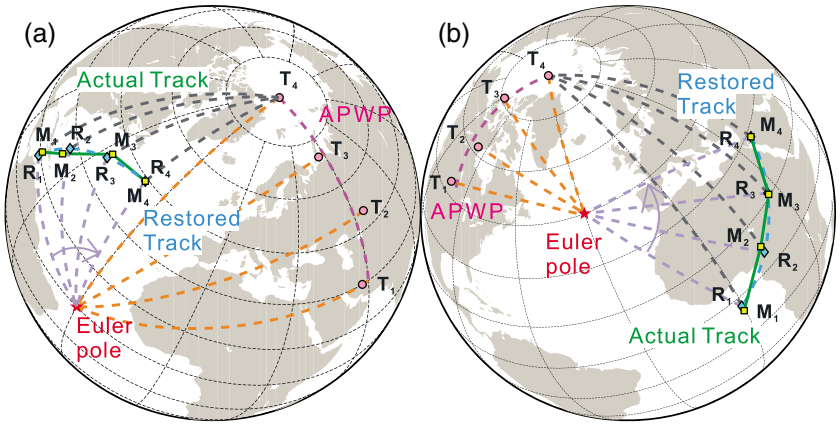

Figure 1. Illustration of absolute plate motion reconstruction from APWP geometric parametrization. Paleomagnetic Euler pole and rotation angle can be computed from either (a) great circle or (b) small circle fitting to an APWP segment ($T_4 - T_1$ with T_1 as the oldest pole). Suppose M_4 (R_4) is a reference site in the current geographic coordinate system which has experienced a rotation during T_1–T_4, the reconstructed locations (R_3 to R_1, cyan diamonds) without correction will deviate from the actual paleopositions (M_3 to M_1, yellow squares). The correction can be made by tracing the great circle distances (paleocolatitudes) along the paleomeridians (black lines) defined by the Earth's spin axis T_4 (stationary) and the initially restored positions R_1–R_4.

On the characterization of the geometry of apparent polar wander path (APWP) for tectonic plate reconstruction, *Francheteau and Sclater* [1969] first attempted to extract rotation axis, i.e., paleomagnetic Euler pole (PEP) from paleomagnetic data sequence. *Gordon et al.* [1984] advanced the application of PEP for plate reconstruction by modeling APWP segments using the best fit small circles. The resulting paleomagnetic Euler parameters (pole position and the corresponding stage rotation angle) are equivalent to those from the fitted hot spot tracks. *Cox and Hart* [1986] expected the comparable predictions from PEP analysis and hot spot frame and a thriving future in applying the PEP method for absolute plate reconstruction back to Precambrian. However, except for a few trials in constructing APWP, not quite successful because of the unjustified assumption of constant plate motion velocity over a geologic duration as long as 10–20 Myr as noted by *Van der Voo* [1993], applying PEP analysis for absolute plate reconstruction still keeps stranded in theory. Still one of the biggest barriers is the relatively low quality of APWPs for most continental plates.

Notably, *Smirnov and Tarduno* [2010] demonstrated the exciting potential of PEP analysis for absolute plate reconstruction by restoring the eruption site of Siberian Permo-Triassic traps back to 250 Ma. Asserting that the great circle parametrization is a more conservative fit to APWP tracks, the authors modeled the tracks using the orientation matrix constructed from the direction cosines of the paleomagnetic poles sequence [*Smirnov and Tarduno*, 2010]. For an APWP segment constituted with less than three poles and with a short overall spherical distance, $<10°$ for instance, the great circle parametrization does appear to provide a sound solution with the minimal changes in plate motion velocity.

It also should be noted that another major concern limiting the widespread application of PEP method for absolute plate reconstruction arises from the discrepancies in the paleomagnetic colatitudes that accumulate between the PEP reconstructions and the paleomagnetic predictions [*Smirnov and Tarduno*, 2010, Supplementary Table 2]. These discrepancies are inevitable in the direct application of the PEP method for plate reconstruction without any correction. This is caused by the fact that actual paleomagnetic data sequence seldom lies perfectly along the modeled great or small circle as is illustrated in Figure 1. To provide a solution to the problem, we suggest to apply a correction to the reconstructions using the paleocolatitudes calculated from the reference site and paleomagnetic poles in the current geographic coordinates frame (Text S2 in the supporting information).

In this paper, we combine both great circle and small circle modeling to extract the paleomagnetic Euler parameters from APWPs. A paleocolatitude correction to the reconstructions is introduced in order to keep the restored paleolatitudes compatible with the paleomagnetic prediction. Using the method, we will

reevaluate the dispersion of East Gondwana since 140 Ma and assess the quality of our technique by comparing our restorations with those from four other paleolongitude determination methods, i.e., fixed hot spot frame [*Müller et al*., 1993], global moving hot spot reference frame [*Doubrovine et al*., 2012], the global hybrid frame [*Torsvik et al*., 2012], and the TPW-derived frame [*Mitchell et al*., 2012].

2. Methods

To extract paleomagnetic Euler parameters (rotation pole and rotation angle) from the identified APWP segments, we combine an iterative algorithm for small circle fitting [*Fisher et al*., 1987] and the orientation matrix method to model the great circle distribution [*Scheidegger*, 1965]. Both great circle and small circle fittings are performed and compared to obtain the better fitting option. The absolute reconstructions are determined using the rotation matrix constructed from the paleomagnetic data along the tracks. To ensure that the reconstructions are compatible with the paleomagnetic predictions, we apply a paleomagnetic colatitude correction to compensate for the discrepancies induced by the deviation of paleomagnetic data from the modeled circle tracks (Figure 1). The uncertainties both for Euler poles and the paleocolatitude corrected reconstructions are then estimated using the modified bootstrap method suggested by *Smirnov and Tarduno* [2010]. For convenience, we present the uncertainty regions in the form of error ellipses, but we note that the true uncertainty regions can be more complicated, with irregular shapes for plate or block contours [cf. *Smirnov and Tarduno*, 2010]. Text S2 in the supporting information provides the detailed description of this synthesized PEP reconstruction method or APWP geometric parameterization (APWPGP).

3. Paleomagnetic Data

Because the reconstructions from the APWPGP method will bear the geological significance only when there is no detectable motion for the paleomagnetically determined Earth's rotation axis (no true polar wander) over the studied time interval, the effect of TPWs on APWP should be corrected before the reconstructions. *Steinberger and Torsvik* [2008] derived four episodes of TPW from the cumulative rotation of all continents around their common mass center in the paleomagnetic reference frame. *Torsvik et al*. [2012] recalculated the magnitude for the four TPWs using the updated paleomagnetic database, based on which they presented the TPW corrected APWPs for the major continental plates. The estimation, however, is valid only under the assumption of nearly zero longitudinal motion of the African plate during the last 320 Ma, which is still open to debate [*Steinberger and Torsvik*, 2008]. *Doubrovine et al*. [2012] transferred the African APWP into their new global moving hot spot frame and attributed the discrepancies between the two frames to be TPW. Note, however, they did not eliminate the possibility that those discrepancies could actually originate from the uncertainties for the assumed plate reconstruction circuits, mantle flow, and hot spot motion models. Therefore, before other TPW corrections can be made to the APWPs employing techniques free of the quasi-stationary African assumption and hot spot-paleomagnetic frames discrepancy, we prefer to use the APWPs without any TPW correction [*Torsvik et al*., 2012] for the absolute plate reconstruction in this work.

4. APWP Geometric Parametrization

Four tracks can be identified for India, Australia, and East Antarctica by trial and modification (Table 1), which were evidenced to be optimal parametrizations by visual inspection (Figure 2), concentration of bootstrap modeled circle centers (Figures S4–S6), and reasonable reconstructions (Figure 4a) comparable to the hybrid reference frames [*Torsvik et al*., 2012]. Facilitated by the paleocolatitude correction for the reconstructions at each age, our APWPGP algorithm saves the trouble of splitting the fit of several continuous APWP segments with minor directional variations, as long as the modeled circle for the dominating APWP segment (usually has a longer spherical distance than the combination of the rest segments) shares the same direction with the overall circle fitting (Figure 2b, Track Ind-1). For APWP tracks with short overall spherical distance ($<10°$), great circle parametrization is preferred (Figure 2c, Track E.Ant-2 and Figure 2d, Track Aus-2) because (1) the direction variations are highly likely caused by the random noise of paleomagnetic data rather than the actual tectonic events, and (2) a geologically unreasonable translation distance might be implied by the usually huge rotations calculated from small circle modeling. For the APWP segments 70–40 Ma of East Antarctica and Australia (Figures 2c and 2d), for instance, small circle modeling would yield to an Euler pole close to the segments with an impractically $>60°$ rotation within 30 Myr, while great circle fitting will present

Table 1. The Calculated Euler Parameters of the Fitted APWP Tracks for India, Australia, and East Antarctica (Figure 2), Which Are Composed of Euler Pole Position (lonE, latE) and the Corresponding Stage Rotation Angle (Ω, Positive for Counterclockwise Rotation Backward in Time)[a]

		Euler Parameters						Rotation Uncertainties			
Track	Period (Ma)	lonE (°E)	latE (°N)	lonE′ (°E)	latE′ (°N)	Ω (deg)	Fitting Code	cov(11) (deg)	cov(12) (deg)	cov(22) (deg)	GCD (deg)
					India						
Ind-1	0–50	15	1.6	15	1.6	25.3	GC	42.13	5.11	1.37	1.37
Ind-2	50–80	14.2	2.9	14.8	3.1	36.2	GC	26.06	1.54	3.83	0.12
Ind-3	80–100	38.9	37.7	56.3	1.4	12.7	GC	237.35	−2.17	3.96	0.18
Ind-4	100–140	27.2	9.7	26.4	1.4	25.5	GC	140.65	−19.46	309.32	4.61
					Australia						
Aus-1	0–40	33.1	0.9	33.1	0.9	18	GC	89.90	10.18	1.99	0.05
Aus-2	40–70	12.1	−4.3	11.5	2.3	10.1	GC	457.67	8.16	5.62	0.19
Aus-3	70–100	112.9	26.8	113.1	−0.9	11.4	GC	254.14	−6.91	5.25	0.15
Aus-4	100–140	72.3	14.2	73.3	0.8	17.3	GC	270.45	7.28	6.61	0.14
					East Antarctica						
E.Ant-1	0–40	39.6	0.9	39.6	0.9	−4.7	GC	2505.30	−130.50	7.90	0.80
E.Ant-2	40–70	358.1	5.6	357.9	2.5	7.2	GC	1015.90	−10.60	20.00	0.70
E.Ant-3	70–100	299.8	-0.4	299.3	1.1	−10.9	GC	335.44	27.40	282.90	3.56
E.Ant-4	100–140	80.8	−2.1	299.3	0.8	14.7	GC	551.31	209.24	675.88	2.54

[a]The corrected Euler poles (lonE′, latE′) used for reconstruction were computed by closing all later rotations. The fitting code represents the best circle modeling method to a certain APWP track, either in great circle (GC) or small circle (SC). The optimal parametrization method was selected based on the concentration of the circle modeling (Figures S4–S6) and the soundness of resulting reconstructions. The corresponding confidence ellipse for each rotation is calculated from the 2 × 2 covariance matrix (cov(21) = cov(12)) which can be constructed from the bootstrapped Euler poles (Figures S10–S12). The great circle distances (GCDs) between the corrected Euler poles and Fisherian means of the bootstrapped data sets are reasonably smaller than 5°, which indicates that the confidence ellipses are good estimation of the rotation errors.

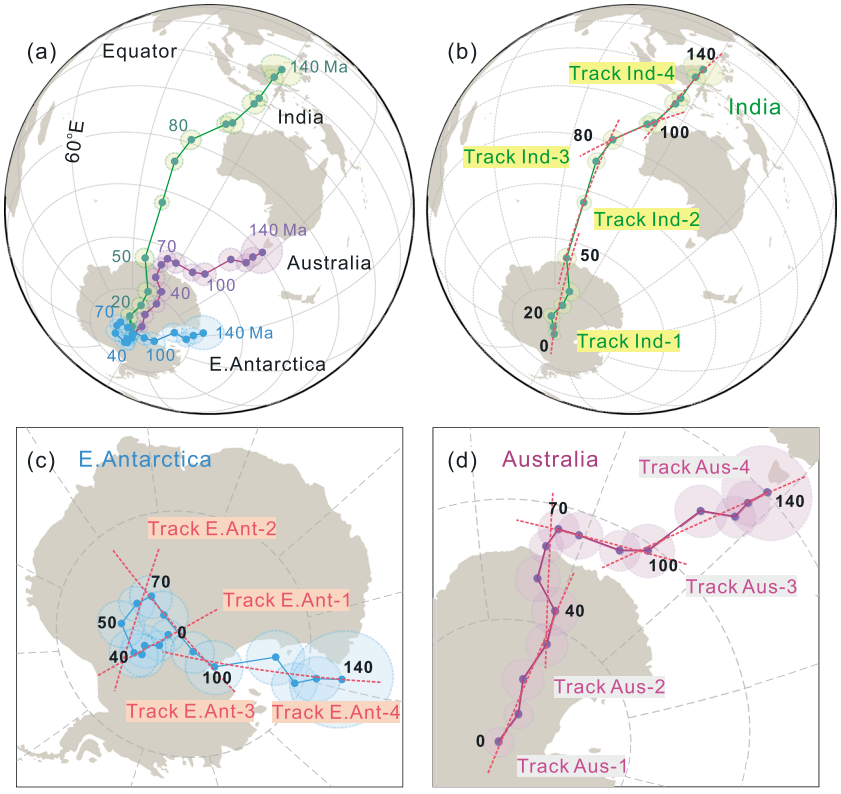

Figure 2. (a) Orthographic projection of the up-to-date 0–140 Ma APWPs for India, Australia, and East Antarctica without true polar wander correction (data are taken from *Torsvik et al.* [2012]). (b–d) The fitted APWP tracks for the plates are indicated as the red dashed lines with the corresponding Euler parameters listed in Table 1.

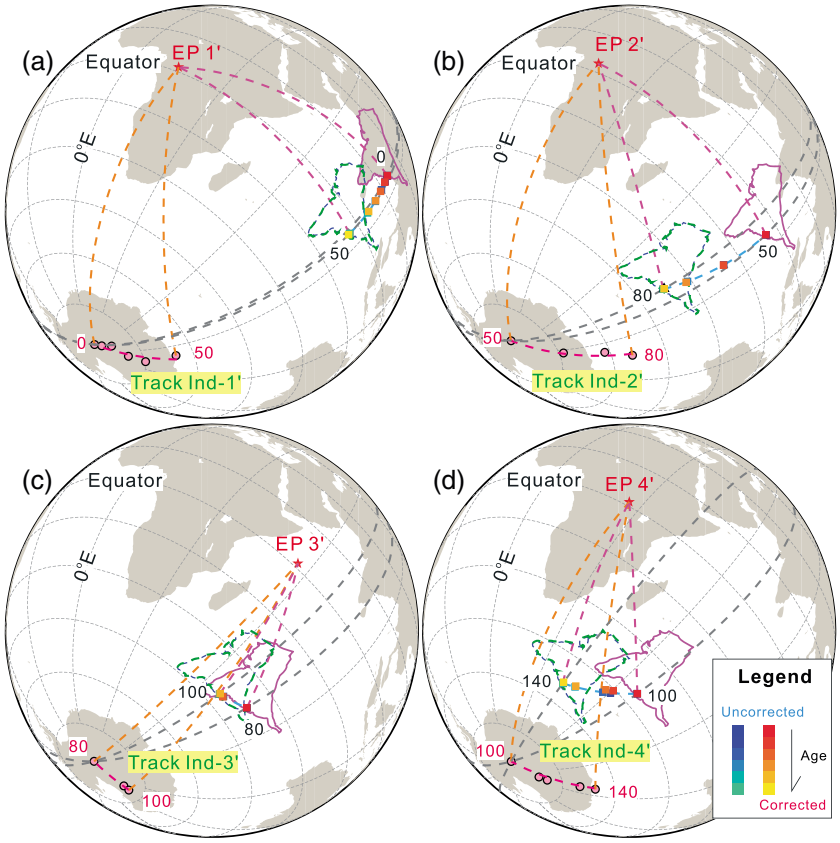

Figure 3. Restoration of India back to 140 Ma. The blue (green) dashed contours represent the restored locations before (after) the paleocolatitude correction and the magenta contour marks the location before rotation. Also shown are the restored paleopositions for the reference site (85°E, 20°N) without (cool colored) and with (warm colored) the paleocolatitude correction along the paleomeridians (black dashed lines). The transferred Euler poles (red star) and APWP tracks (pink dash line) are also illustrated.

a more reliable rotation consistent with the published plate tectonic models [e.g., *Whittaker et al*., 2013]. However, the final decision for the optimal parametrization choice could be made only after obtaining reasonable reconstructions from the candidate Euler parameters. The reconstructions from other absolute plate motion frames (e.g., hot spots and slab remnants frames) and the age distribution of world oceanic crust can always be used in assisting this decision making process.

All the paleomagnetic Euler parameters as well as the corresponding APWP tracks for the studied continents were transferred into the geographic coordinates frame of the latest pole (0 Ma) by closing the later rotations using the APWPGP algorithm described above (Figures 3, S1, and S2). For absolute plate reconstruction, we used the present-day recognizable contours for the three continents. The reconstructions (of the reference sites) corrected for paleocolatitude do not show much discrepancies with those without correction, which indicates the soundness of the circle fittings. To estimate the confidence regions for each restoration, we constructed 100 bootstrap resampled paleomagnetic pole sequences from the original Indian, Australian, and East Antarctic APWPs (Figure S3). Both great and small circle parameters were computed from the 100 new APWPs during the same time intervals for the identified tracks (Figures S4–S6). The scattering of modeled Euler poles are used as an additional affirmation for selecting the optimal circle parametrization method. Since the ultimate goal of uncertainty analysis is to evaluate the confidence regions for the reconstructed reference site or plate rather than the errors in the Euler parameters, we emphasize the quantifications and visualization of the uncertainty ellipses for the 100 iterations of paleolatitude-corrected reconstructions (Figures 4a, 4b, and S7–S9 and Table S2). The confidence areas for the transferred Euler poles are estimated in the same way in our study (Figures S10–S12 and Table 1).

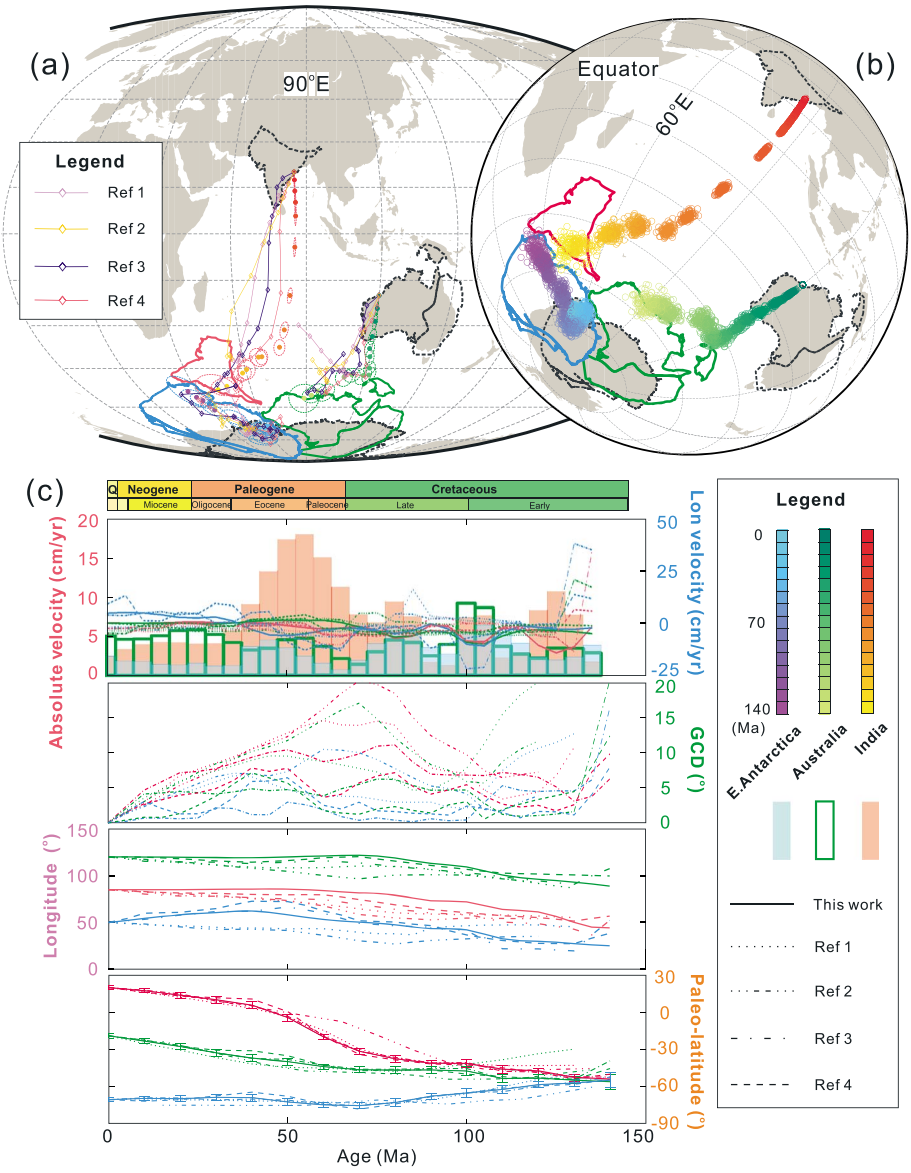

Figure 4. (a) Reconstructed East Gondwana configuration for India (red), Australia (green), and East Antarctica (light blue) at 140 Ma. The motion trajectories for the references sites (color-coded circles) with uncertainties are calculated in 10 Myr interval (Table S2). Also shown are the reconstructions in 10 Myr interval calculated from four other published reference models for comparison. (b) Bootstrapped reconstructions for the reference sites (100 times repetitions), from which the uncertainty ellipses are computed. (c) The absolute motion velocities (stack bars) and longitudinal velocities (lines), great circle distances between the predictions from the APWPGP method and other reference frame models, longitudinal displacement, and paleolatitude movement (error bars are computed from TPW uncorrected APWPs of *Torsvik et al.* [2012]) with time are computed for the selected reference sites from the interpolation of the reconstructions in 5 Myr interval. The published models used for the comparison are the following: *Müller et al.* [1993] (Ref 1), *Doubrovine et al.* [2012] (Ref 2), *Mitchell et al.* [2012] (Ref 3), and *Torsvik et al.* [2012] (Ref 4).

5. Discussion and Conclusions

Our reconstructions indicate that India experienced a northeastward translation and a rapid counterclockwise (~50° counterclockwise (CCW)) rotation with respect to the meridians during 140–100 Ma (Figures 3d and S13). After a mostly eastward drift during 100–80 Ma, there was a much faster rate of climbing in latitude with an average speed of ~12 cm/yr (the top rate of ~18 cm/yr between 60 and 70 Ma) and ~20° CCW rotation during 80–50 Ma (Figure 4c), when the collision between India and Eurasia at ~50 Ma largely

decreased its northward convergence [*Molnar et al*., 2010]. *Cande and Stegman* [2011] suspected that the hasty acceleration and deceleration might be correlated with the force of the Réunion plume head during 67–52 Ma.

According to the reconstructions, Australia appears to have experienced ~30° CCW rotation with respect to the meridians in the past 140 Myr (Figure S1). The transition from eastward to mostly northward motion occurred at ~70 Ma for Australia with a jump in its translation direction and speed (~8–9 cm/yr) during 110–100 Ma (Figures 4b, 4c, and S13). East Antarctica also bore a primarily east sense of drift and CCW rotation during 140–70 Ma before it switched into slow northwestward (70–40 Ma, ~2.8 cm/yr), and then southwestward (40–0 Ma, ~1.5 cm/yr) drift with the accompanied CW rotation (Figures 4b, 4c, S2, and S13).

Notably, our reconstructions shown in Figures 4 and S13 indicate within uncertainties that India-East Antarctica affinity might be broken down by the West Enderby Basin spreading ridge around 130–120 Ma [*Gaina et al*., 2007] rather than a later age of 118–90 Ma [*Jokat et al*., 2010]. Our results also suggest that the breakup between Australia and India might occur during 130–120 Ma (Figure S13c), corresponding to the spreading in the Gascoyne and Cuvier Abyssal Plains initiated at ~132 Ma [*Seton et al*., 2012, and references therein]. Our results indicate a closely synchronized (with only a slight deviation) plate motion direction and speed between Australia and East Antarctica during ~140–80 Ma, and that Australia drifted northward progressively with an average speed of 4 cm/yr until reaching its current location (Figures 4, S13b, and S13c). Our observations are consistent with the previous relative plate motion studies. *Ball et al*. [2013], for instance, suggested the bound between the two plates finally broke up at ~53 Ma after an eastward propagation of rifting (165–83 Ma) and the subsequent seafloor spreading (83–53 Ma). *Whittaker et al*. [2013] identified a major change in relative motion direction between Australia and East Antarctica between 108 and 100 Ma, which, however, is slightly later than our 110 Ma "kink" (Figures 2c, 2d, and S13). Considering that the confidence regions of the APWPs is a statistic calculation and can be enlarged or decreased by using new poles with higher quality, our reconstructions cannot eliminate possibility that the two kinks are the same or related until new high-quality paleomagnetic poles are published. We caution that all the tectonic interpretations above are drawn under the assumption that the studied APWPs are accurate, which nevertheless is not guaranteed for the paleomagnetic data within or close to the Cretaceous Normal Superchon (CNS, ~ 120–80 Ma) where age assignment for some data is still questionable [*Besse and Courtillot*, 2002]. Future work is needed to improve the accuracy of APWPs during CNS by updating the paleomagnetic database.

To further evaluate the robustness and limitations of our APWPGP method, we compare our reconstructions with those from four other absolute plate motion reference frames with different derivation techniques: fixed hot spot reference frame (FHRF) [*Müller et al*., 1993], global moving hot spot reference frame (GMHRF) [*Doubrovine et al*., 2012], the TPW-derived reference frame (TPWRF) [*Mitchell et al*., 2012] and global hybrid reference frame (GHRF) [*Torsvik et al*., 2012]. In overall, the three continents exhibit an eastward translation in longitude (Figure 4c) but the specific forms are quite different. To assess the potential reasons for this observation in terms of paleomagnetism, we calculate the expected paleolatitude drift (EPD) for the selected reference sites during 0–140 Ma using the APWPs without TPW correction of *Torsvik et al*. [2012] which are compared with the paleolatitude corresponding to the reconstructions using different models (Figure 4c). Model FHRF and GMHRF have statistically significant deviations from the EPD during 50–140 Ma, while TPWRF, GHRF, and our APWPGP model show a generally similar trend in paleolatitude evolution. Similar observation can be made from the great circle distance (GCD) plot for the three continents, which are smaller than 10° but can reach as large as ~15–25° for India and Australia during 50–100 and 130–140 Ma for model FHRF and GMHRF (Figure 4c). Such first-order ineffectiveness for model FHRF and GMHRF in terms of paleolatitude prediction can be attributed to the episodes of TPW during 50–140 Ma, inadequate accuracy of the APWPs without TPW correction or the limited robustness of hot spot models. Further studies in paleomagnetism and geodynamic models are needed to better account for this observation. In contrast, model TPWRF and GHRF show relatively small deviations from EPD except for a few time intervals and are thus close to our model in terms of reconstructions (GCD $<$ ~10°). We will focus on the comparison with these two models in further discussion.

In general, our APWPGP method shows the most similarity in reconstructions with GHRF except a few trivial deviations. Compared with the predictions from GHRF, our reconstructions do not reveal a communal

southward translation of the three East Gondwana continents during 140–130 Ma. However, this movement is still within the confidence regions for our reconstructions (Figures 4a and 4b) despite a sudden augment in the spherical distance during 140–130 Ma (Figure 4c). The primary cause for the discrepancies between the GHRF and our APWPGP technique lies in that the former reconstructions were made based on the TPW corrected paleomagnetic data under the quasi-stationary Africa assumption, which still needs confirmation from other evidence independent of the GHRF. A similarly small great circle distance discrepancies can be observed between ours and TPWRF (Figure 4c), which is reasonable because this frame was constructed by slightly shifting the longitude of the reconstructions of *Torsvik et al*. [2008a] to align the minimum moment of inertia with the suggested current geoid highs [*Pavoni*, 2008]. In contrast, the reconstruction from the slab remnant frame deviates more from ours at 140 Ma where they rotated East Gondwanaland as a unity ~40° CCW when the seafloor spreading among the three continents already initiated [*van der Meer et al*., 2010, Supplementary Figure 34]. The discrepancies might root from the over westward correction to the anchor slab material in the model of *van der Meer et al*. [2010], as is disapproved by the recent reassessment of the same slab reference frame by *Butterworth et al*. [2014] through comparing the modeled slab positions with the observed slab positions in mantle tomography.

We note that there are several limitations for the application of the APWPGP method: (1) the high requirement and dependency for the accuracy of the studied APWP(s); (2) the likely small reconstruction errors caused by the discrepancies among the geographic coordinates of 0 Ma paleomagnetic poles among APWPs of different continents; (3) exhaustive data processing sometimes for tracing the somewhat subjectively decided optimal circle modeling option which is most reasonably fitted to the existing geologic evidence; (4) that there might be indiscernible plate motion in the case of pure east-westward translation with respect to Earth's spin axis, i.e., no recorded paleomagnetic polar wandering; and (5) that the confidence region calculated here only describes the statistical uncertainties accumulated through each step of computation for the optimal fitting option. Despite the limitations, APWPGP method exhibits a great potential in quantifying absolute plate motions applicable back to Late Paleozoic as long as there are reliable APWPs.

Acknowledgments

The apparent polar wander paths used in the paper are from *Torsvik et al*. [2012]. Data supporting Figure 4 are available in Table S2 in the supporting information. The study was partially funded by the Natural Sciences and Engineering Research Council of Canada (NSERC) of V.K. We thank Compute/Calcul Canada for granting us access to the West Grid computational facility. The paper benefitted greatly from the comments and suggestions of R.D. Müller and two anonymous reviewers.

The Editor thanks R. Dietmar Muller and an anonymous reviewer for their assistance in evaluating this paper.

References

Ball, P., G. Eagles, C. Ebinger, K. McClay, and J. Totterdell (2013), The spatial and temporal evolution of strain during the separation of Australia and Antarctica, *Geochem. Geophys. Geosyst.*, *14*, 2771–2799, doi:10.1002/ggge.20160.

Besse, J., and V. Courtillot (2002), Apparent and true polar wander and the geometry of the geomagnetic field over the last 200 Myr, *J. Geophys. Res.*, *107*(B11), 2300, doi:10.1029/2000JB000050.

Butterworth, N. P., A. S. Talsma, R. D. Müller, M. Seton, H.-P. Bunge, B. S. A. Schuberth, G. E. Shephard, and C. Heine (2014), Geological, tomographic, kinematic and geodynamic constraints on the dynamics of sinking slabs, *J. Geodyn.*, *73*, 1–13.

Cande, S. C., and D. R. Stegman (2011), Indian and African plate motions driven by the push force of the Réunion plume head, *Nature*, *475*(7354), 47–52.

Cox, A., and R. B. Hart (1986), *Plate Tectonics: How it Works*, Blackwell Scientific Publications, Inc., Boston, Mass.

Doubrovine, P. V., B. Steinberger, and T. H. Torsvik (2012), Absolute plate motions in a reference frame defined by moving hot spots in the Pacific, Atlantic, and Indian oceans, *J. Geophys. Res.*, *117*, B09101, doi:10.1029/2011JB009072.

Fisher, N. I., T. Lewis, and B. J. Embleton (1987), *Statistical Analysis of Spherical Data*, Cambridge Univ. Press, Cambridge, U. K.

Francheteau, J., and J. Sclater (1969), Paleomagnetism of the southern continents and plate tectonics, *Earth Planet. Sci. Lett.*, *6*(2), 93–106.

Gaina, C., R. D. Müller, B. Brown, T. Ishihara, and S. Ivanov (2007), Breakup and early seafloor spreading between India and Antarctica, *Geophys. J. Int.*, *170*(1), 151–169.

Gordon, R. G., A. Cox, and S. O'Hare (1984), Paleomagnetic Euler poles and the apparent polar wander and absolute motion of North America since the Carboniferous, *Tectonics*, *3*(5), 499–537, doi:10.1029/TC003i005p00499.

Jokat, W., Y. Nogi, and V. Leinweber (2010), New aeromagnetic data from the western Enderby Basin and consequences for Antarctic-India break-up, *Geophys. Res. Lett.*, *37*, L21311, doi:10.1029/2010GL045117.

Mitchell, R. N., T. M. Kilian, and D. A. Evans (2012), Supercontinent cycles and the calculation of absolute palaeolongitude in deep time, *Nature*, *482*(7384), 208–211.

Molnar, P., W. R. Boos, and D. S. Battisti (2010), Orographic controls on climate and paleoclimate of Asia: Thermal and mechanical roles for the Tibetan plateau, *Annu. Rev. Earth Planet. Sci.*, *38*(1), 77–102.

Morgan, W. J. (1971), Convection plumes in the lower mantle, *Nature*, *230*, 42C43.

Müller, R. D., J.-Y. Royer, and L. A. Lawver (1993), Revised plate motions relative to the hotspots from combined Atlantic and Indian Ocean hotspot tracks, *Geology*, *21*(3), 275–278.

O'Neill, C., D. Müller, and B. Steinberger (2005), On the uncertainties in hot spot reconstructions and the significance of moving hot spot reference frames, *Geochem. Geophys. Geosyst.*, *6*, Q04003, doi:10.1029/2004GC000784.

Pavoni, N. (2008), Present true polar wander in the frame of the Geotectonic Reference System, *Swiss J. Geosci.*, *101*(3), 629–636.

Scheidegger, A. E. (1965), On the statistics of the orientation of bedding planes, grain axes, and similar sedimentological data, *U.S. Geol. Surv. Prof. Pap.*, *525*, 164–167.

Seton, M., et al. (2012), Global continental and ocean basin reconstructions since 200 Ma, *Earth Sci. Rev.*, *113*(3), 212–270.

Smirnov, A. V., and J. A. Tarduno (2010), Co-location of eruption sites of the Siberian Traps and North Atlantic Igneous Province: Implications for the nature of hotspots and mantle plumes, *Earth Planet. Sci. Lett.*, *297*(3), 687–690.

Steinberger, B., and T. H. Torsvik (2008), Absolute plate motions and true polar wander in the absence of hotspot tracks, *Nature*, *452*(7187), 620–623.
Tarduno, J. A. (2007), On the motion of Hawaii and other mantle plumes, *Chem. Geol.*, *241*(3), 234–247.
Torsvik, T. H., R. D. Müller, R. Van der Voo, B. Steinberger, and C. Gaina (2008a), Global plate motion frames: Toward a unified model, *Rev. Geophys.*, *46*, RG3004, doi:10.1029/2007RG000227.
Torsvik, T. H., B. Steinberger, L. R. M. Cocks, and K. Burke (2008b), Longitude: Linking Earth's ancient surface to its deep interior, *Earth Planet. Sci. Lett.*, *276*(3), 273–282.
Torsvik, T. H., et al. (2012), Phanerozoic polar wander, palaeogeography and dynamics, *Earth Sci. Rev.*, *114*(3–4), 325–368.
van der Meer, D. G., W. Spakman, D. J. van Hinsbergen, M. L. Amaru, and T. H. Torsvik (2010), Towards absolute plate motions constrained by lower-mantle slab remnants, *Nat. Geosci.*, *3*(1), 36–40.
Van der Voo, R. (1993), *Paleomagnetism of the Atlantic, Tethys and Iapetus Oceans*, Cambridge Univ. Press, New York.
Whittaker, J. M., S. E. Williams, and R. D. Müller (2013), Revised tectonic evolution of the Eastern Indian Ocean, *Geochem. Geophys. Geosyst.*, *14*, 1891–1909, doi:10.1002/ggge.20120.

Auxiliary Material for Paper 2014GL060080

Derivation of paleo-longitude from the geometric parametrization of apparent polar wander path: implication for absolute plate motion reconstruction

Lei Wu and Vadim A. Kravchinsky
Department of Physics, University of Alberta, Edmonton, Alberta, Canada T6G 2E1.

Introduction

The Auxiliary Material includes a text detailing the methods, two data tables, thirteen figures and two movies.

The auxiliary material contain
1. 2014GL060080-sup-0001-readme.txt (ReadMe Text): Description of the content of supplementary materials.

2. 2014GL060080-sup-0002-Text.docx (Supplementary Text). Supplementary tables, supplementary figures and captions, movie captions as well as the corresponding reference.

3. 2014GL060080-sup-0003-ms01.avi (Supplementary Movie 1). Absolute plate reconstruction of East Gowdwana (India, Australia and East Antarctica) dispersion since 140 Ma (forward in time).

4. 2014GL060080-sup-0004-ms02.avi (Supplementary Movie 2). Absolute plate reconstruction of East Gowdwana (India, Australia and East Antarctica) dispersion during 0 - 140 Ma (backward in time).

Appendix A: Supplementary materials

Supplementary materials include a text detailing the methods, two data tables, thirteen figures and two movies.

Derivation of paleo-longitude from the geometric parametrization of apparent polar wander path: implication for absolute plate motion reconstruction

Lei Wu [1*] and Vadim A. Kravchinsky [1]

1 – Department of Physics, University of Alberta, Edmonton, Alberta, Canada T6G 2E1

** – Corresponding author: Tel: +1-(780)-4925591; Fax: +1-(780)-4920714; E-mail:* lwu2@ualberta.ca

Geophysical Research Letters

2014

Supplementary Text:

A1. Parametrization of APWP tracks

To parametrize the APWP segments in terms of paleomagnetic Euler parameters (stage rotation pole and rotation angle), Gordon et al. [1984] proposed a global search technique to find the circle centers from the best fitted small circles. This numerical approach, however, converges on the optimal solutions slowly. To improve the efficiency of data fitting process, we apply an iterative algorithm summarized by Fisher et al. [1987], which aims to seek the optimal small circle center $\hat{\Lambda}'(x, y, z)$ (row vector in Cartesian coordinate system) by minimizing the sum of the squares of angular distance (ψ_i) from the individual poles $\hat{\lambda_i}'(l_i, m_i, n_i)$ (direction cosines) to the circle center.

$$(l_i, m_i, n_i)\begin{pmatrix} x \\ y \\ z \end{pmatrix} = \cos\psi_i$$

To start the iterative procedure, an initial estimate of the circle center needs to be made. For unification, we used the Fisherian mean pole $\widehat{\Lambda_0}'(x_0, y_0, z_0)$ for the paleomagnetic data set.

$$x_0 = \frac{\sum_{i=1}^{k} l_i}{R}, y_0 = \frac{\sum_{i=1}^{k} m_i}{R}, z_0 = \frac{\sum_{i=1}^{k} n_i}{R}$$

$$R = \sqrt{\left(\sum_{i=1}^{k} l_i\right)^2 + \left(\sum_{i=1}^{k} m_i\right)^2 + \left(\sum_{i=1}^{k} n_i\right)^2}$$

where R is magnitude of the resultant vector.

Repeat the following calculations until the difference between the last two iterates $\left(\hat{\Lambda}^{(j)}, \psi^{(j)}\right)$ and $\left(\hat{\Lambda}^{(j-1)}, \psi^{(j-1)}\right)$ are reasonably small (we choose 1×10^{-5} degree in our program), where *j* is the iteration number:

$$\tan\psi_j = \frac{\sum_{i=1}^{k}\sqrt{\left[1-\left(\lambda_i'\hat{\Lambda}_{j-1}\right)\right]}}{R}, \qquad \hat{\Lambda}_j = \frac{Y}{\sqrt{Y'Y}}$$

where i = 1, 2, ..., n, and

$$\mathrm{Y} = \cos\psi_j \sum_{i=1}^{k}\lambda_i - \sin\sum_{i=1}^{k} X_i\,, \qquad X_i = \frac{\left(\hat{\lambda}_i'\hat{\Lambda}_{j-1}\right)\hat{\lambda}_i - \hat{\Lambda}_{j-1}}{\sqrt{1-\left(\hat{\lambda}_i'\hat{\Lambda}_{j-1}\right)^2}}$$

Note that the great circle center can be obtained using this technique by setting ψ_i to be 90°. For comparison purpose, we applied an alternative algorithm from Scheidegger [1965] to model the great circle distribution using orientation matrix **T** which can be constructed from the paleomagnetic poles:

$$T = \begin{pmatrix} \sum l_i \cdot l_i & \sum l_i \cdot m_i & \sum l_i \cdot n_i \\ \sum m_i \cdot l_i & \sum m_i \cdot m_i & \sum m_i \cdot n_i \\ \sum n_i \cdot l_i & \sum n_i \cdot m_i & \sum n_i \cdot n_i \end{pmatrix}$$

The pole to a particular polar wander segment can then be calculated as the eigenvector corresponding to the minimum eigenvalue of the orientation matrix **T**. The discrepancy between the great circle centers calculated from the two methods is statistically insignificant but we used the orientation matrix for great circle modelling throughout this work.

The stage rotation angles Ω_i subtending the fitted APWP tracks can be computed from

$$\Omega_i = \cos^{-1}\frac{\cos s - \cos \mathrm{p}_1 \cos \mathrm{p}_2}{\sin \mathrm{p}_1 \sin \mathrm{p}_2}$$

where s, p_1 and p_2 present the angular distance between the starting and ending paleomagnetic poles, the starting pole and Euler pole, and the ending pole and Euler pole, respectively. For unification, we assign the positive sign for the counterclockwise rotation backward in time, 0-40 Ma for instance.

To quantify the confidence region for the modelled Euler parameters $(\hat{\Lambda}_i, \Omega_i)$, we modified the bootstrap method recommended by Smirnov and Tarduno [2010]. 1) Treat each individual paleomagnetic pole along the modelled tracks as a discrete Fisherian distribution, which can be re-sampled 100 times using the precision parameter for the pole [Fisher et al., 1981]. 2) Construct a new APWP $\left(\hat{\lambda}^{(1)}, \hat{\lambda}^{(2)}, \ldots, \hat{\lambda}^{(n)}\right)$ by randomly selecting one data-point from each distribution, from which both great and small circle Euler parameters $\left((\hat{\Lambda}_{GC}^{(1)}, \Omega_{GC}^{(1)}), (\hat{\Lambda}_{SC}^{(1)}, \Omega_{SC}^{(1)})\right)$ can be calculated for the selected time interval. 3) Repeat the previous steps for another 99 times to obtain the dataset $\left\{((\hat{\Lambda}_{GC}^{(1)}, \Omega_{GC}^{(1)}), (\hat{\Lambda}_{SC}^{(1)}, \Omega_{SC}^{(1)})), ((\hat{\Lambda}_{GC}^{(2)}, \Omega_{GC}^{(2)}), (\hat{\Lambda}_{SC}^{(2)}, \Omega_{SC}^{(2)})), \ldots, ((\hat{\Lambda}_{GC}^{(100)}, \Omega_{GC}^{(100)}), (\hat{\Lambda}_{SC}^{(100)}, \Omega_{SC}^{(100)}))\right\}$. 4) Calculate the confidence ellipses at 0.05 significance level from the covariance matrix either from great circle or small circle center.

To facilitate the choice of better parametrization (great or small circle fitting) for a certain APWP track on the first order, we computed the variance ratio V_r introduced by Gray et al. [1980],

$$V_r = (k-3)\frac{\mathrm{r}_g - \mathrm{r}_s}{\mathrm{r}_s}$$

where r_g and r_s represent the sums of the squares of the angular residuals for great and small circle fitting respectively. The significant improvement of the small circle modelling over the great circle fitting can be tested at 0.05 significance level by comparing V_r with $F_{1,n-3}$ assuming that r_g and r_s are normally distributed [Gray et al., 1980].

It should be cautioned that the parametrization of a whole APWP is a relatively subjective task and there might be several alternative fitting combinations that appear to be equally reasonable both visually and quantitatively. In other words, the seemingly perfect fitting results are entirely possible to present questionable plate reconstructions either in the plate translation velocity or in the restored paleo-longitude compared with other absolute plate motion reference frames. The two primary reasons are 1) the still limited accuracy of APWPs owing to the inadequate quantity and quality of

paleomagnetic poles and the kinematic models used to transfer poles during certain time intervals such as in the Cretaceous Normal Superchron [Besse and Courtillot, 2002] and 2) the possible shift of the whole Earth relative to its spin axis [e.g., Mitchell et al., 2012]. Therefore, the premier selection rule for the optimal circle modelling combination is to obtain a geologically sound reconstruction which in practice requires many trials and modifications.

A2. Absolute plate reconstruction from paleomagnetic Euler parameters

For absolute plate motion reconstruction, we construct rotation matrices R_i from the modelled paleomagnetic Euler parameters $(\hat{\Lambda}_i, -\Omega_i)$ where negative sign before the rotation angles signifies restoration (backward rotation in time which is opposite to the directions for the calculation of stage rotation angle) [Cox and Hart, 1986].

$$R_i = \begin{pmatrix} x_i x_i(1-\cos\Omega_i)+\cos\Omega_i & x_i y_i(1-\cos\Omega_i)+z_i\sin\Omega_i & x_i z_i(1-\cos\Omega_i)-y_i\sin\Omega_i \\ y_i x_i(1-\cos\Omega_i)-z_i\sin\Omega_i & y_i y_i(1-\cos\Omega_i)+\cos\Omega_i & y_i z_i(1-\cos\Omega_i)+x_i\sin\Omega_i \\ z_i x_i(1-\cos\Omega_i)+y_i\sin\Omega_i & z_i y_i(1-\cos\Omega_i)-x_i\sin\Omega_i & z_i z_i(1-\cos\Omega_i)+\cos\Omega_i \end{pmatrix}$$

The geographic coordinates of a reference point $\hat{P}_j^{\,t}$ on a sphere before rotation can be calculated using the following matrix multiplication:

$$\hat{P}_j^{\,t} = R_i \hat{P}_j$$

where $\hat{P}_j = (a_j^1, a_j^2, a_j^3)$ represents the same reference point after rotation.

Because actual APWPs usually consist of more than one segment, the Euler poles subtended to the earlier tracks must be transferred into the frame of the Earth's spin axis defined by the latest paleomagnetic pole (the present day pole at 0 Ma). In other words, earlier stage rotation poles $\hat{\Lambda}_i^{\,t}$ used for reconstruction must be calculated by closing all the later rotations, whose procedure is comparable to that of using stage poles fitted from magnetic anomalies and fracture-zone crossings [e.g., Kirkwood et al., 1999]. This can be achieved by combine rotations using matrix multiplication [Cox and Hart, 1986]:

$$\hat{\Lambda}_i^{\,t} = R_{i-1} R_{i-2} \cdots R_1 \hat{\Lambda}_i$$

Accordingly, all the paleomagnetic poles $\left(\widehat{\lambda_1^J}, \widehat{\lambda_2^J}, \ldots, \widehat{\lambda_n^J}\right)$ along earlier APWP tracks can be transferred in the same manner for the purpose of our proposed paleo-colatitude correction.

$$\left(\widehat{\lambda_1^J}^t, \widehat{\lambda_2^J}^t, \ldots, \widehat{\lambda_k^J}^t\right) = R_{i-1}R_{i-2}\cdots R_1\left(\widehat{\lambda_1^J}, \widehat{\lambda_2^J}, \ldots, \widehat{\lambda_k^J}\right)$$

To ensure the absolute paleo-position reconstructions compatible with those from the paleomagnetic frame, we apply a paleomagnetic colatitude correction to compensate for the discrepancies induced by the deviation of paleomagnetic data from the modelled circle tracks (Figure 1). Assuming there is no shift of the Earth's spin axis (represented by the latest paleomagnetic pole along each transferred APWP track in the geocentric axial dipole model) with respect to the mantle, the corrected reconstructions can be obtained by tracing great circle arcs (i.e., the paleo-meridians) from the spin axis to the endpoints. The great circle arcs, i.e. the paleomagnetic colatitudes, are calculated as the spherical distance between the reference site and paleomagnetic poles in the current geographic coordinate frame.

A3. Uncertainty analysis

To provide the uncertainties for the reconstructed paleo-positions, we construct another 100 APWPs using bootstrap resampling technique suggested by Smirnov and Tarduno [2010], where each paleomagnetic pole with the corresponding uncertainty A_{95} will be treated as a distinct Fisherian distribution. 100 new sets of Euler parameters are calculated for the same identified time intervals (or tracks) and 100 new sets of reconstructions for the reference site can be determined using the same method described above. Note that a minimum of 100 times bootstrap resampling is required for well-resolved APWPs with 95% confidence ovals no larger than 5°. For APWPs with larger uncertainties, however, more iterations are recommended.

To quantify and visualize the uncertainty bounds for the bootstrapped Euler poles and reconstructions which at this stage lacking explicit understanding about the underlying probability density function, we undertake a conservative estimation to the error regions

using ellipses on a first order. The error shapes are expected to be more complex if the plate (or block) contour rather than a single reference point is used for reconstructions, whose error bounds can be contoured as is advocated by Smirnov and Tarduno [2010]. In this study, we opt to estimate the true confidence regions using ellipses. For this, a simplified chi-square test is performed at the significance level of 0.05 to the bootstrapped rotation parameters and the corresponding reconstructed positions, similar to the treatment described by Gordon et al. [1984]. Under the assumption that the bootstrapped data sets still follow Fisherian distribution, $(\hat{X}_i - \bar{X})$ form chi-square distributions with 2 degrees of freedom (i.e., latitude and longitude), where $\hat{X}_i$ is the *i*th bootstrap coordinates in the data pool (Euler pole or reconstruction) with the Fisherian mean being $\bar{X}$ ($\bar{X}$ can also be the fitted Euler poles and reconstructions from the main procedure). Two dimensional covariance matrix can be constructed from each bootstrap data group, with the maximum (minimum) eigenvector characterizing the major (minor) semi-axis of the confidence ellipse. The limitation for this error characterization is that the bounds are not straightforward to summarize in tabular form so users need to calculate the bounds from the covariance matrices.

We note that the Euler poles and reconstructions calculated from the main procedure do not necessarily equal to the Fisherian means of the bootstrapped data sets. The discrepancy between the two approaches zero when the repetition of bootstrap sampling are infinitely large which however, will significantly increase the amount of computation time. In practice, we consider the discrepancy to be insignificant when the spherical distance is no larger than 5° and thus characterize the uncertainty region of the Euler poles and the corresponding reconstructions by transferring the elliptical semi-axes centered on the Fisherian means of bootstrap datasets directly to to them (Table 1, Supplementary Table 2). We also note that deviations from the Fisherian distributions for reconstructions accumulate back into the oldest times and that the possibility of larger such deviations can be expected for the reconstructions derived from other APWPs with different geometries.

Supplementary Table 1. Transferred APWP segments for reconstruction purpose by rotating earlier APWP segments into the geographic frame of the first poles (0 Ma).

India			Australia			E.Antarctica		
Age (Ma)	lonP (°N)	latP (°E)	Age (Ma)	lonP (°N)	latP (°E)	Age (Ma)	lonP (°N)	latP (°E)
0	353.9	-88.5	0	353.9	-88.5	0	353.9	-88.5
10	60.4	-87.2	10	119.3	-86.6	10	319.7	-87.3
20	74.7	-83.7	20	113.0	-82.2	20	325.9	-85.6
30	101.7	-79.7	30	121.4	-77.1	30	314.9	-84.9
40	106.8	-74.7	40	119.5	-72.9	40	320.0	-84.1
50	98.4	-65.1						
			40	-7.6	-88.5	40	-5.7	-88.5
50	4.5	-87.0	50	54.4	-84.9	50	33.1	-85.2
60	94.0	-73.6	60	80.9	-82.0	60	61.1	-83.6
70	96.8	-61.5	70	93.4	-80.3	70	75.7	-82.7
80	101.9	-54.2						
			70	352.8	-88.5	70	354.5	-88.4
80	1.8	-87.6	80	234.9	-88.4	80	251.9	-88.2
90	136.2	-81.0	90	214.9	-83.2	90	221.5	-83.2
100	139.9	-79.2	100	206.0	-79.9	100	213.9	-80.3
100	-0.9	-87.7	100	0.9	-88.6	100	-2.2	-88.5
110	110.8	-82.1	110	145.8	-82.8	110	144.4	-84.2
120	112.5	-79.5	120	164.4	-79.3	120	172.7	-82.1
130	111.8	-69.9	130	160.2	-77.0	130	167.4	-79.7
140	112.8	-65.5	140	159.9	-74.0	140	167.1	-76.7

Supplementary Table 2. The reconstructed paleo-positions and corresponding uncertainties for the reference sites (lonR, latR) in India, Australia and East Antarctica during 0–140 Ma. The confidence ellipses at each time are calculated from the 2 × 2 covariance matrix (cov(21)=cov(12)) which can be constructed from the bootstrapped data group (Figure 4a, b, Figure S10-12). The small great circle distance (GCD) between the reconstructions and Fisherian means of the bootstrapped data sets (<2º) indicates that the confidence ellipses are reasonably sound estimation of the reconstruction errors.

	India						East Antarctica					
Age (Ma)	lonR (°E)	latR (°N)	cov(11) (°)	cov(12) (°)	cov(22) (°)	GCD (°)	lonR (°E)	latR (°N)	cov(11) (°)	cov(12) (°)	cov(22) (°)	GCD (°)
0	85	20	0	0	0	0	50	-70	0	0	0	0
10	85.2	17.4	0.05	-0.42	5.78	0.1	54.3	-69.1	44.26	3.35	6.34	0.26
20	85.4	13.8	0.05	-0.46	8.27	0.08	58.2	-69.4	60.51	6.28	9.88	0.3
30	85.7	10.1	0.07	-0.3	9.53	0.07	60.5	-68.4	75.72	3.54	10.47	0.35
40	85.8	5.7	0.09	0.04	8.61	0.09	62.1	-68.7	79.39	1.64	9.48	0.36
50	85.5	-4.3	0.17	0.45	9.51	0.09	58.2	-72.1	82.98	4.29	10.44	0.22
60	83.3	-20	1.08	1.16	6.59	0.09	53.1	-74.3	111.87	3.03	7.24	0.19
70	80.4	-31.5	3.6	2.07	7.84	0.11	50.3	-74.9	179.28	6.8	7.52	0.27
80	77.8	-37.5	6.56	1.12	7.83	0.11	47.4	-72.3	138.2	-8.98	9.16	0.23
90	69.1	-40.9	8.45	1.48	7.44	0.13	43.5	-67.1	61.08	-7.5	9.28	0.25
100	67.5	-41	16.45	-0.16	10.37	0.13	42	-64.4	55.99	-3.78	11.29	0.36
110	60.5	-45.5	20.42	3.64	12.56	0.65	32.5	-61.4	35.02	-8.28	11.38	0.28
120	58.1	-46.8	21.36	3.96	8.19	0.77	29.7	-57.4	37.07	-1.79	8.81	0.17
130	47.6	-51.8	76.45	9.93	11.93	1.19	27.4	-56.1	45.42	-5.51	10.57	0.19
140	42	-53.1	119.89	-0.56	35.3	1.31	24.9	-53.8	67.66	-13.92	36.34	0.41
				Australia								
0	120	-20	0	0	0	0						
10	119.8	-24.3	0.14	0.14	5.19	0.19						
20	119.6	-28.6	0.74	0.42	7.43	0.2						
30	119.4	-33.8	2.46	0.96	7.23	0.24						
40	119.1	-38	4.78	0.02	7.25	0.26						
50	120	-40.9	4.09	-1.3	7.59	0.24						
60	121.1	-45	7.17	0.32	6.04	0.22						
70	121.7	-47.5	9.88	1.79	8.17	0.18						
80	118.9	-47.8	15.38	2.4	9.95	0.28						
90	113.1	-47.5	17.03	0.18	6.65	0.23						
100	109.	-48.3	19.3	-0.9	11.1	0.29						
110	100.6	-54.1	23.86	4.68	11.3	0.24						
120	96.1	-53.6	25.31	1.56	8.56	0.19						
130	93	-55.3	26.68	0.58	8.08	0.23						
140	88.8	-56.5	75.21	1	31.9	0.33						

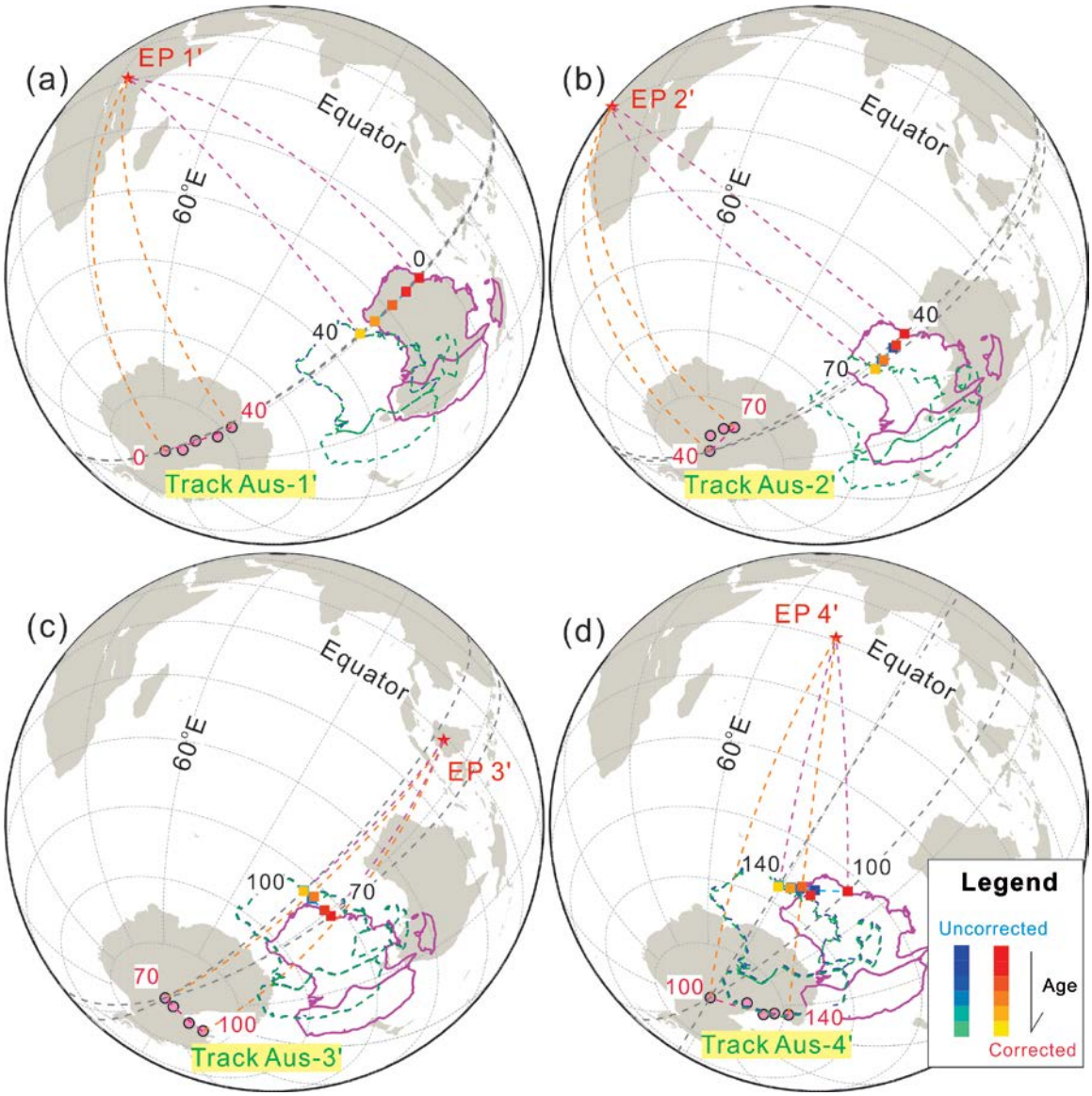

Supplementary Figure 1. Reconstruction of Australia back to 140 Ma ago using our APWP geometric parameterizaiton (APWPGP) method. The earlier Euler poles and corresponding APWP tracks were transferred by closing later rotations. See the main text for detailed description. All the markers and color schemes are the same as the Figure 3 in the main text.

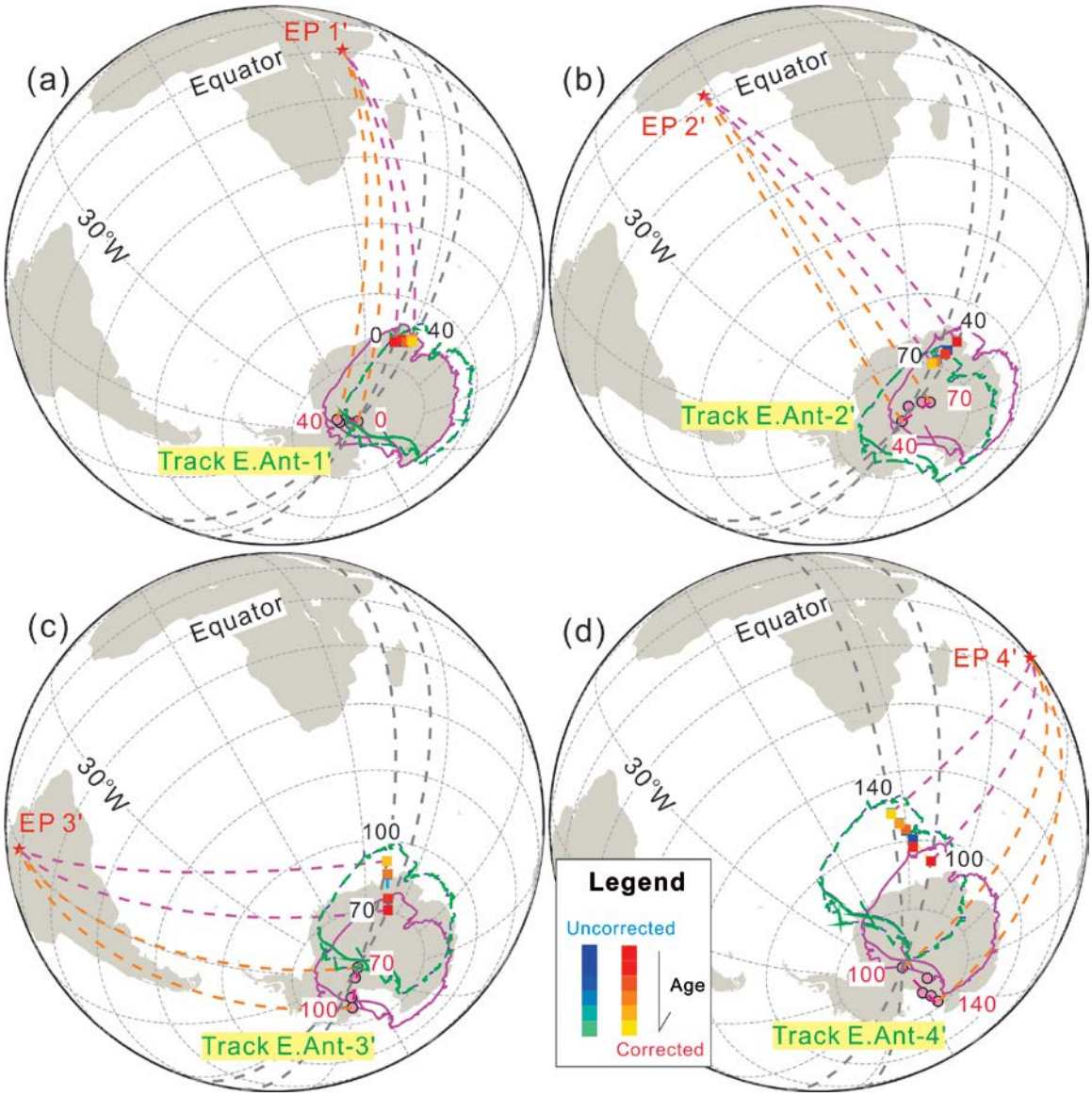

Supplementary Figure 2. Reconstruction of East Antarctica in the past 140 Ma using our APWPGP method. The earlier Euler poles and corresponding APWP tracks were transferred by closing later rotations. See the main text for detailed description. All the markers and color schemes are the same as the Figure 3 in the main text.

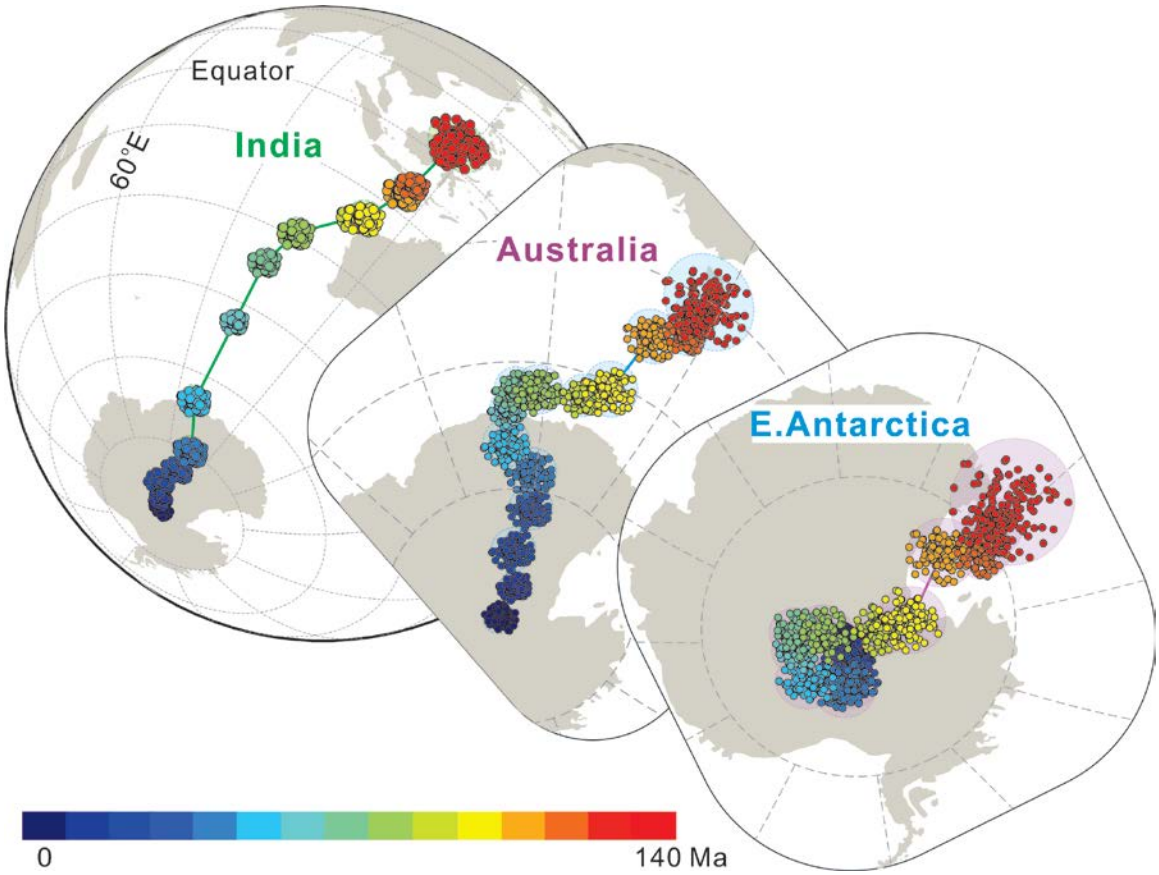

Supplementary Figure 3. Bootstrap resampled data (100 times) from the original paleomagnetic data sequence for India, Australia and East Antarctica using precision parameters K [Fisher et al., 1981], which were estimated from 95% confidence cones provided by Torsvik et al. [2012].

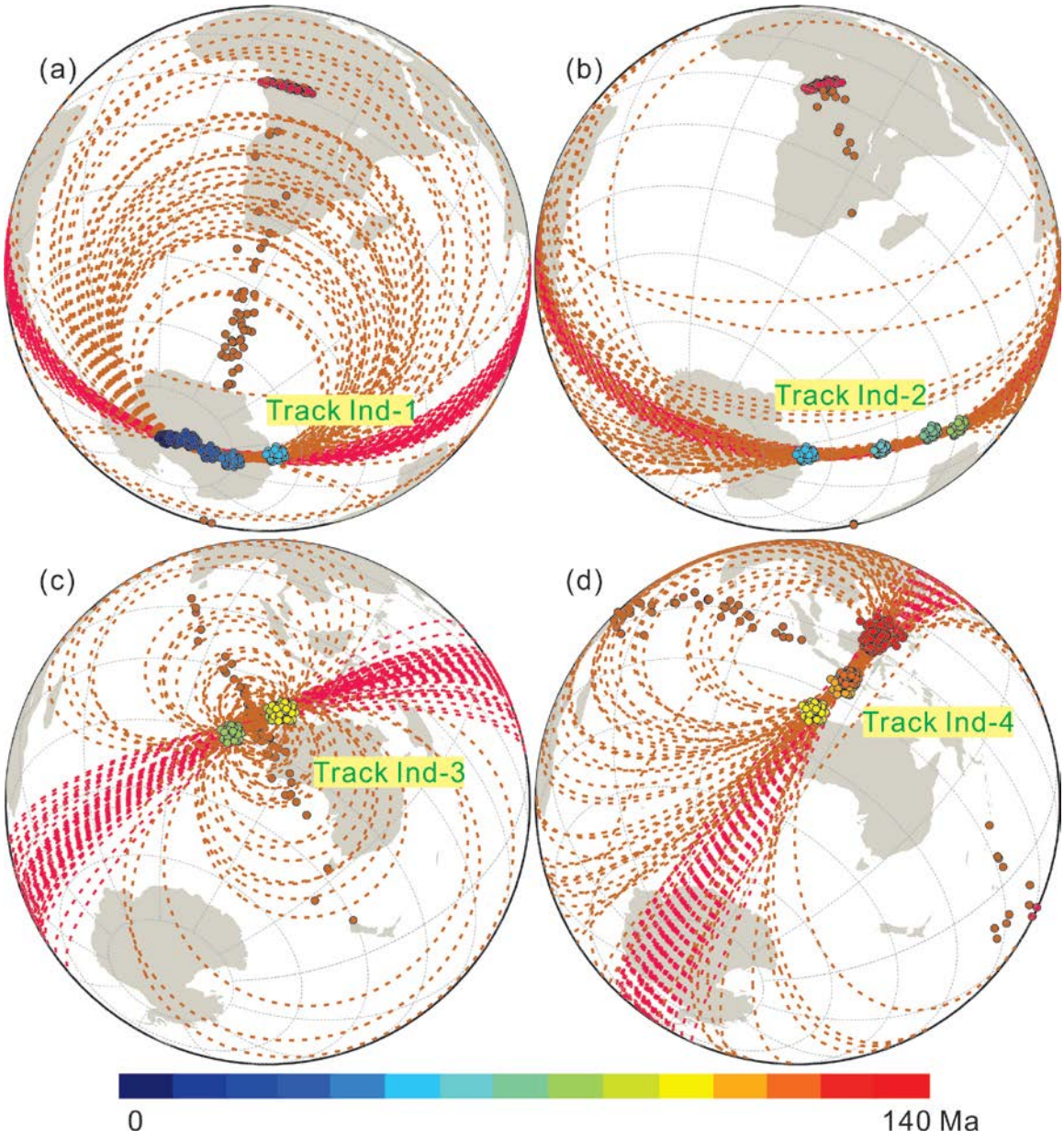

Supplementary Figure 4. Bootstrapped great circle (red dashed circles and dots as the poles) and small circle (bronze dashed circles and dots) parametrization process to the resampled paleomagnetic data sequences (50 times) which correspond to the four selected Indian APWP tracks (Table 1). The concentration of modelled circle centers is used for assisting the optimal fitting method selection.

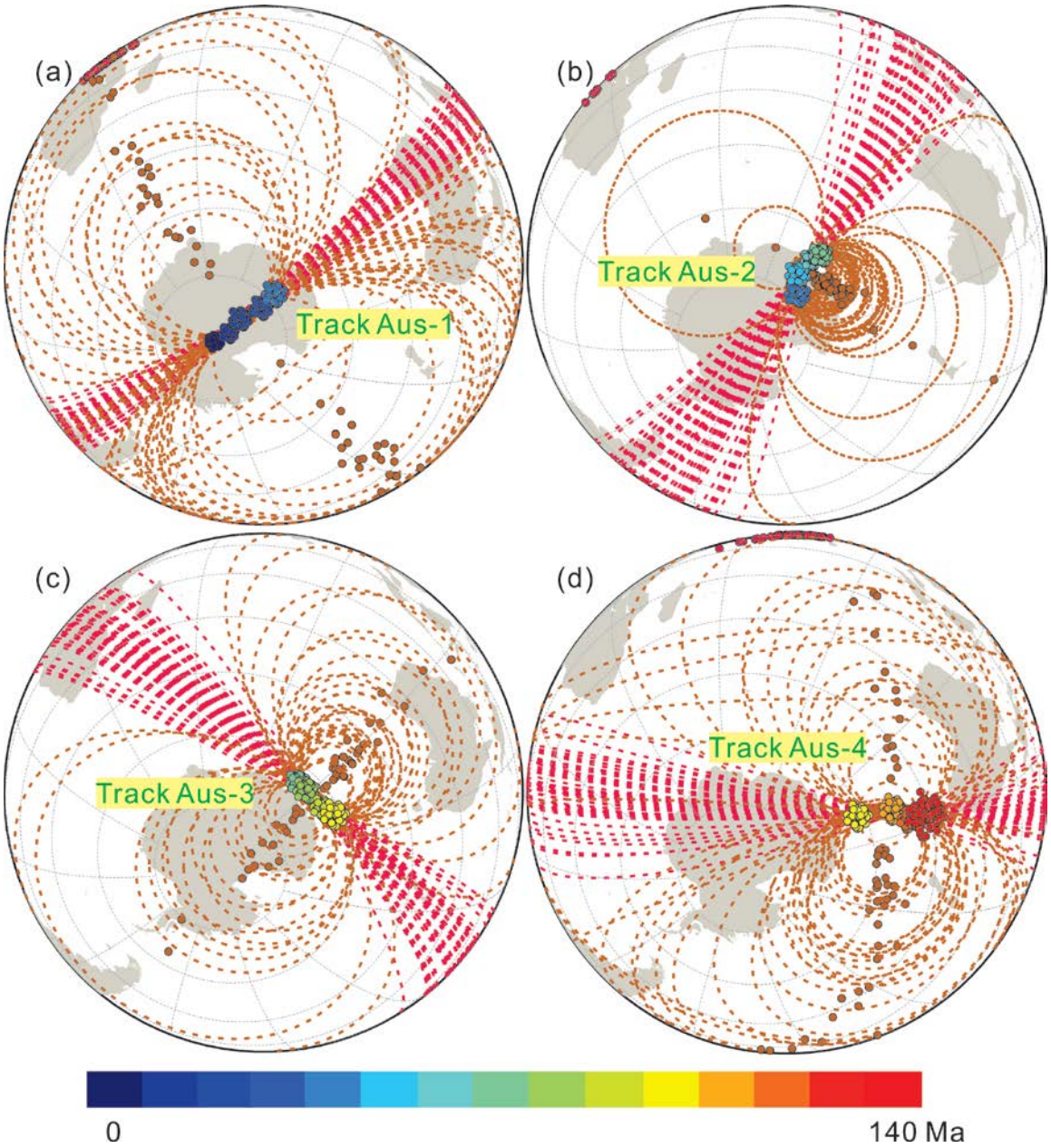

Supplementary Figure 5. Bootstrapped great circle and small circle parametrizations (50 times) for the identified Australian APWP tracks (Table 1). The scattering of the resulting poles can be used as indicator for choosing the better fitting option.

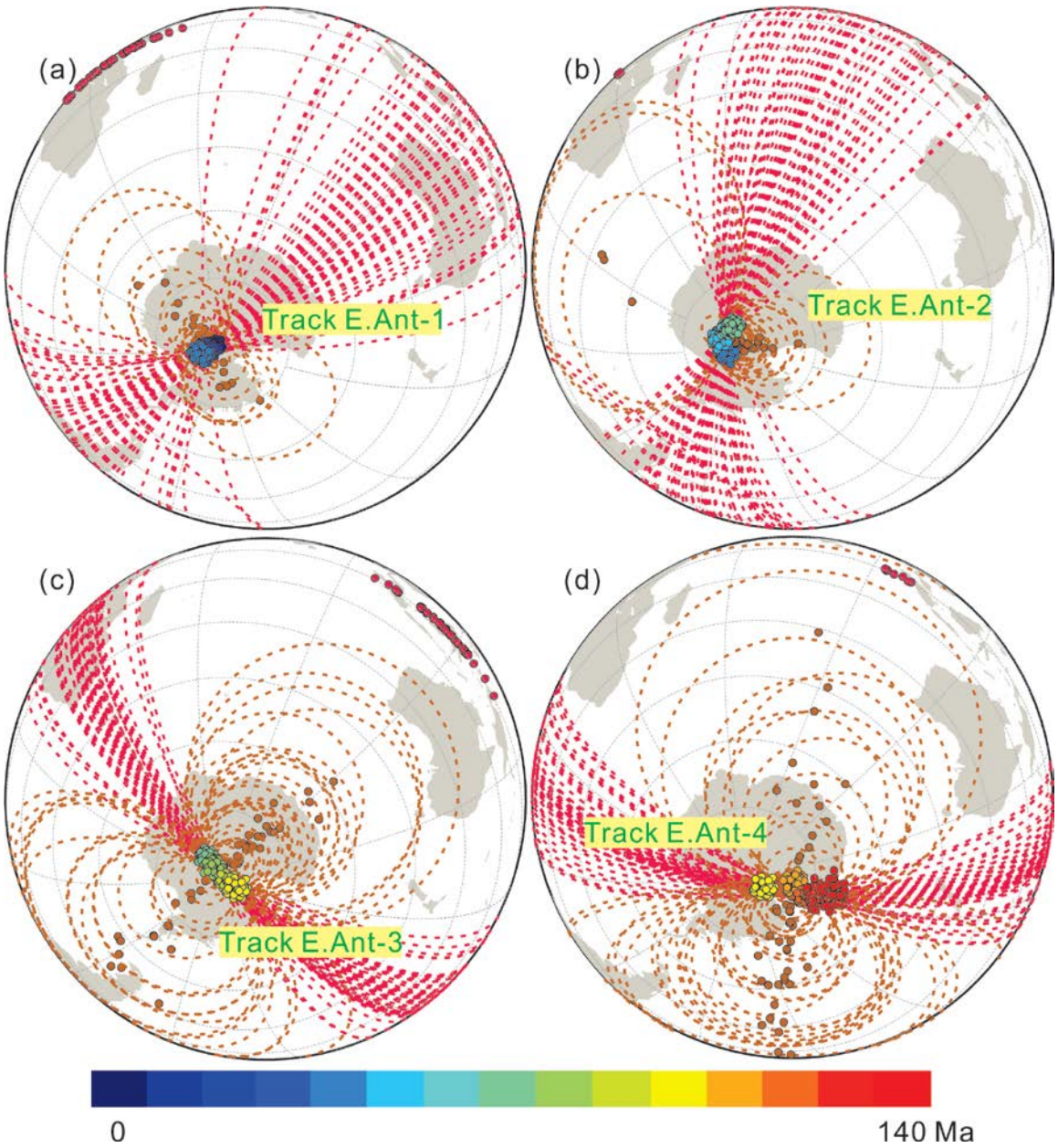

Supplementary Figure 6. Bootstrapped great circle and small circle parametrizations (50 times) for East Antarctica (Table 1). The scattering of the resulting poles can be used as indicator for choosing the better fitting option.

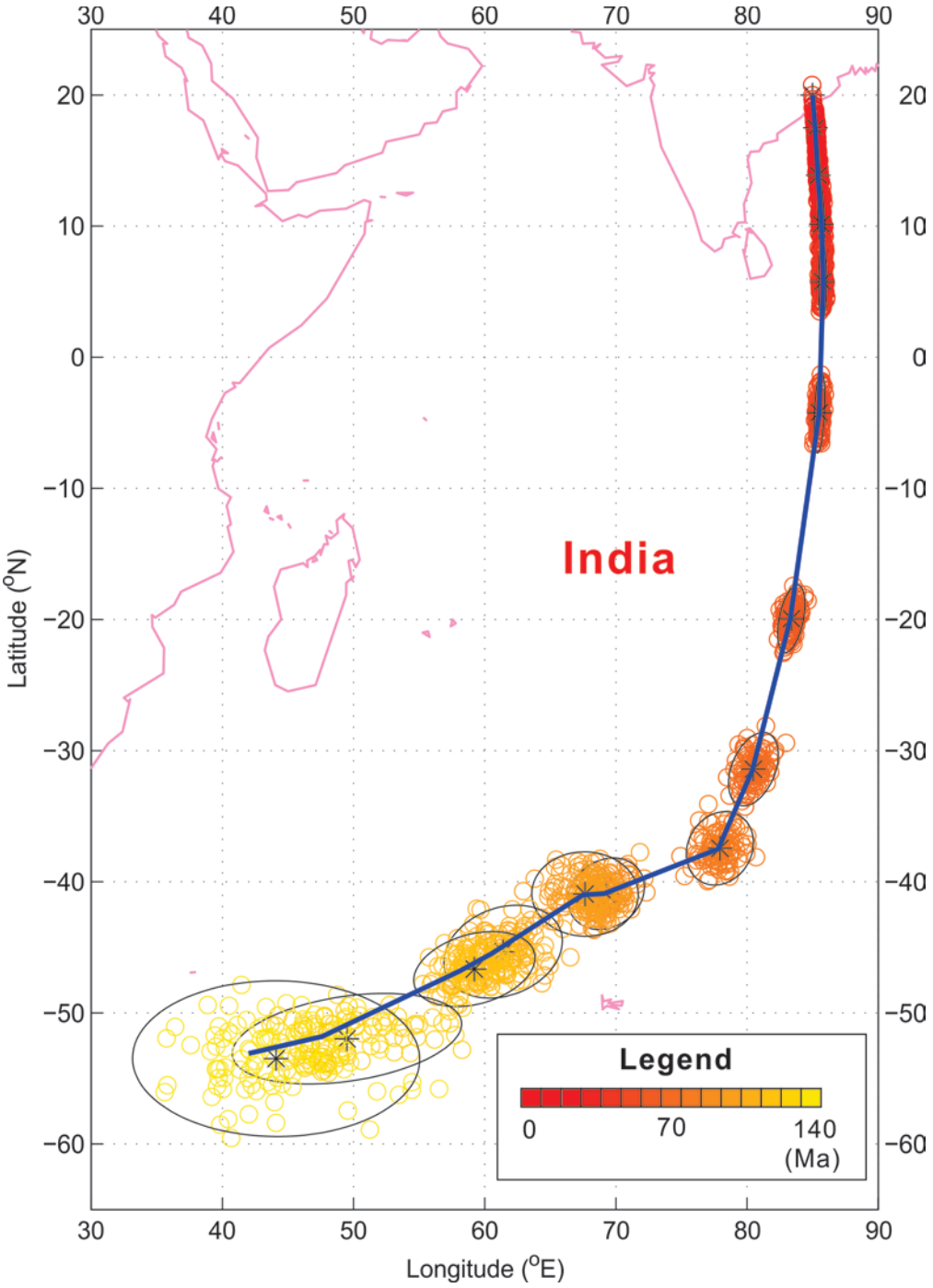

Supplementary Figure 7. Uncertainty ellipses for the bootstrapped reconstructions for India since 140 Ma. The covariance matrices used for characterizing the ellipses are listed in Table S2. Black stars are the Fisherian means for each data set and the blue line represent the reconstructed motion trajectory of the reference site.

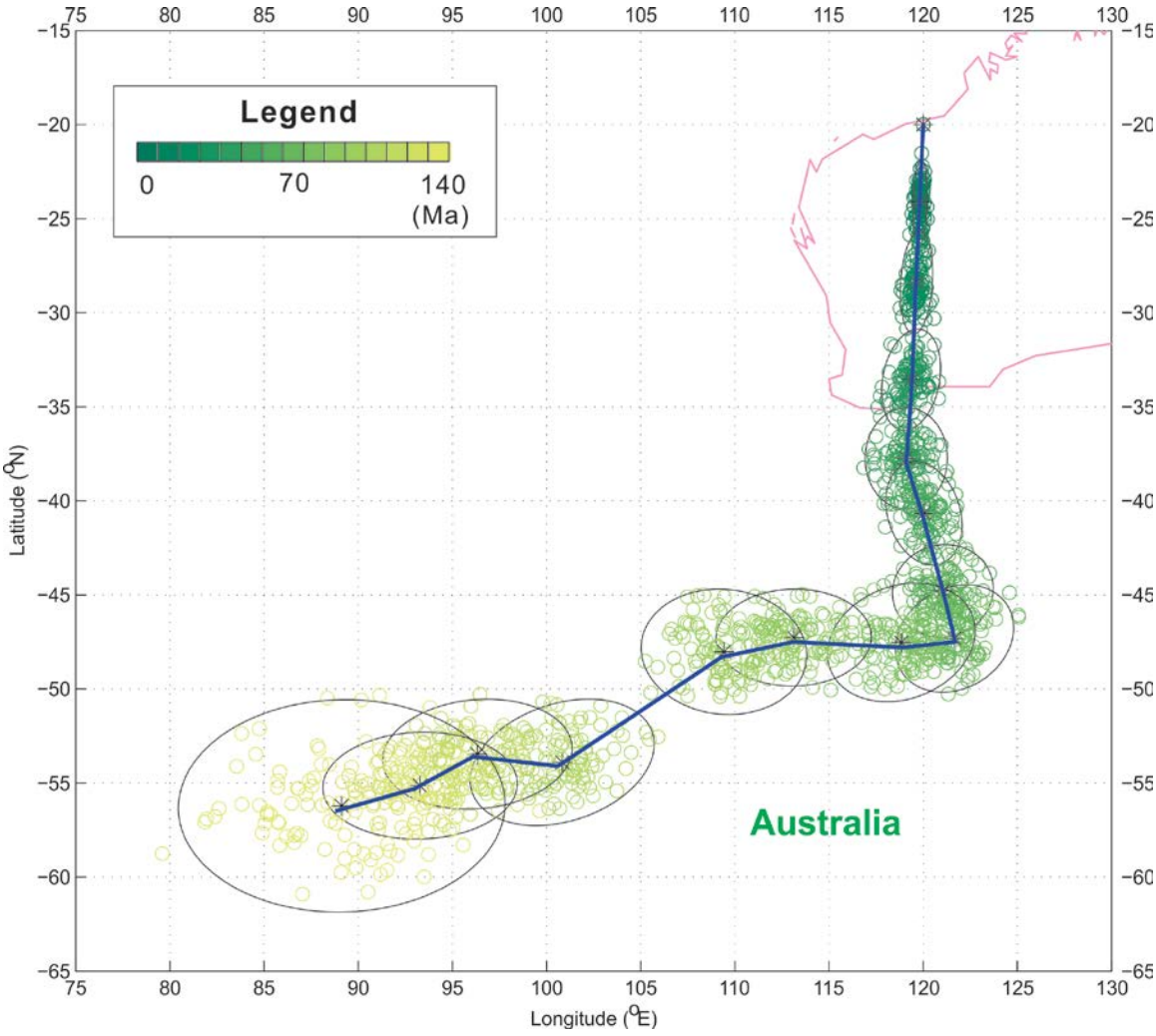

208

209 **Supplementary Figure 8.** Uncertainty ellipses for the bootstrapped reconstructions for
210 Australia since 140 Ma. The covariance matrices used for characterizing the ellipses are
211 listed in Supplementary Table 2. Black stars are the Fisherian means for each data set and
212 the blue line represent the reconstructed motion trajectory of the reference site.

213

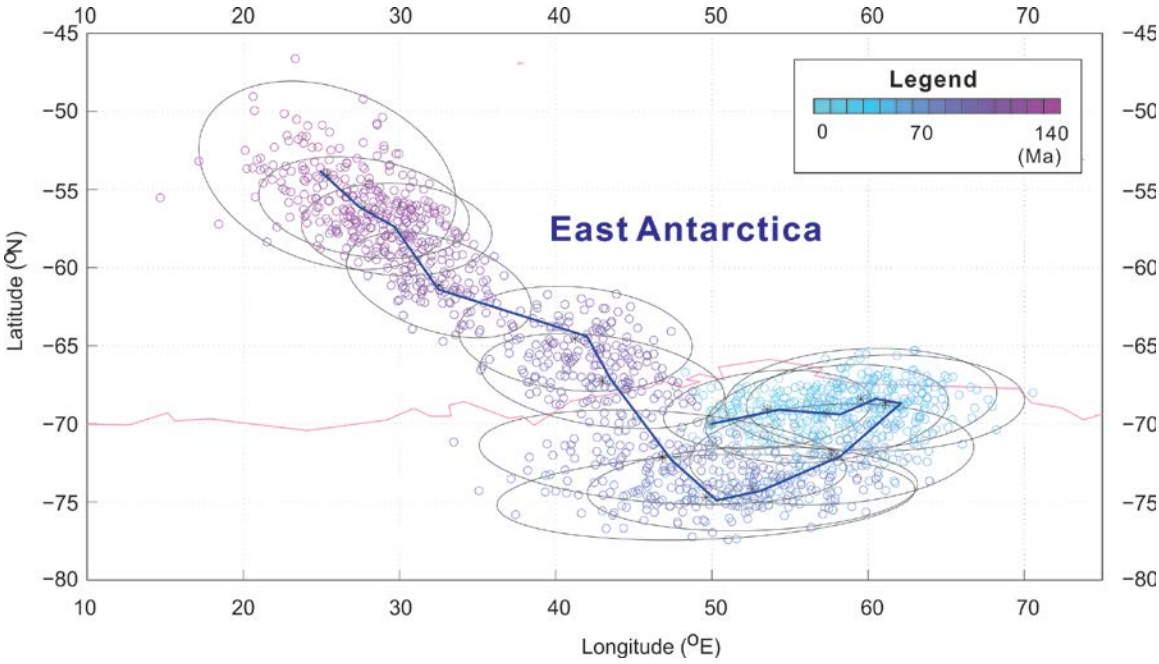

Supplementary Figure 9. Uncertainty ellipses for the bootstrapped reconstructions for East Antarctica since 140 Ma. The covariance matrices used for characterizing the ellipses are listed in Table S2. Black stars are the Fisherian means for each data set and the blue line represent the reconstructed motion trajectory of the reference site.

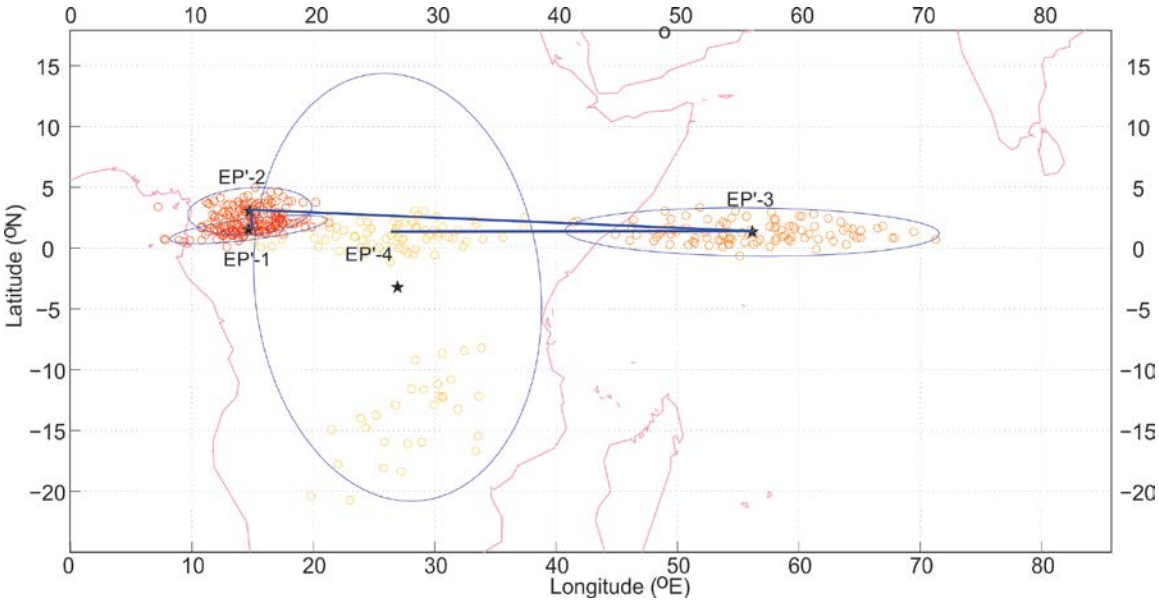

Supplementary Figure 10. Uncertainty ellipses of the bootstrapped Euler pole positions for the identified Indian APWP tracks. The covariance matrices used for characterizing the ellipses are listed in Table 1. Black stars are the Fisherian means for each data set and the blue line represent the trajectory of the rotation poles.

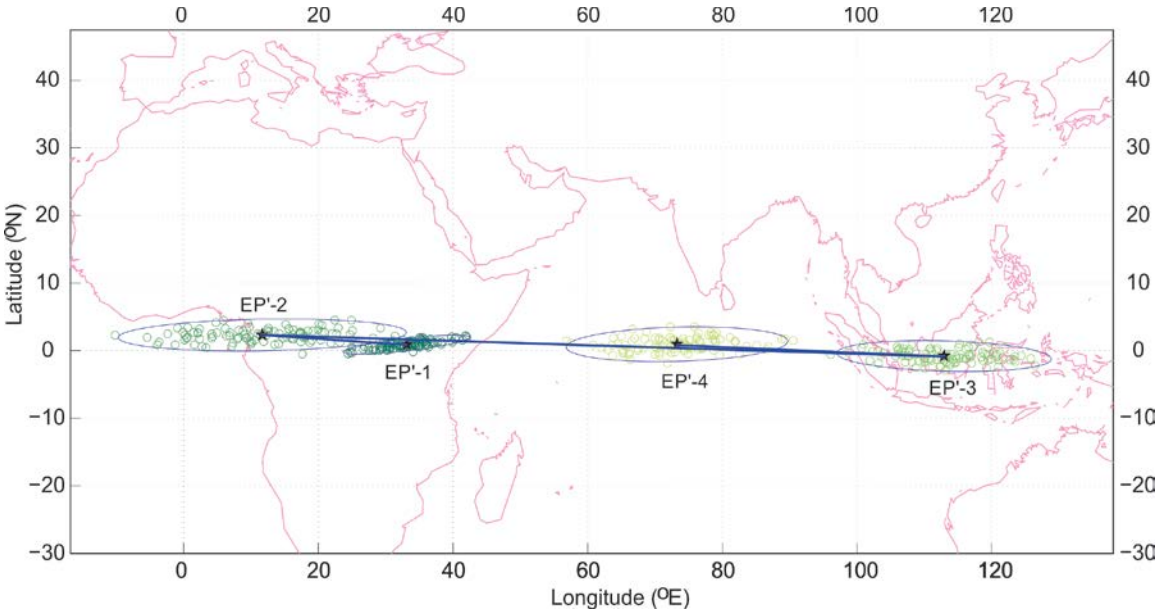

Supplementary Figure 11. Uncertainty ellipses of the bootstrapped Euler pole positions for the identified Australian APWP tracks. The covariance matrices used for characterizing the ellipses are listed in Table 1. Black stars are the Fisherian means for each data set and the blue line represent the trajectory of the rotation poles.

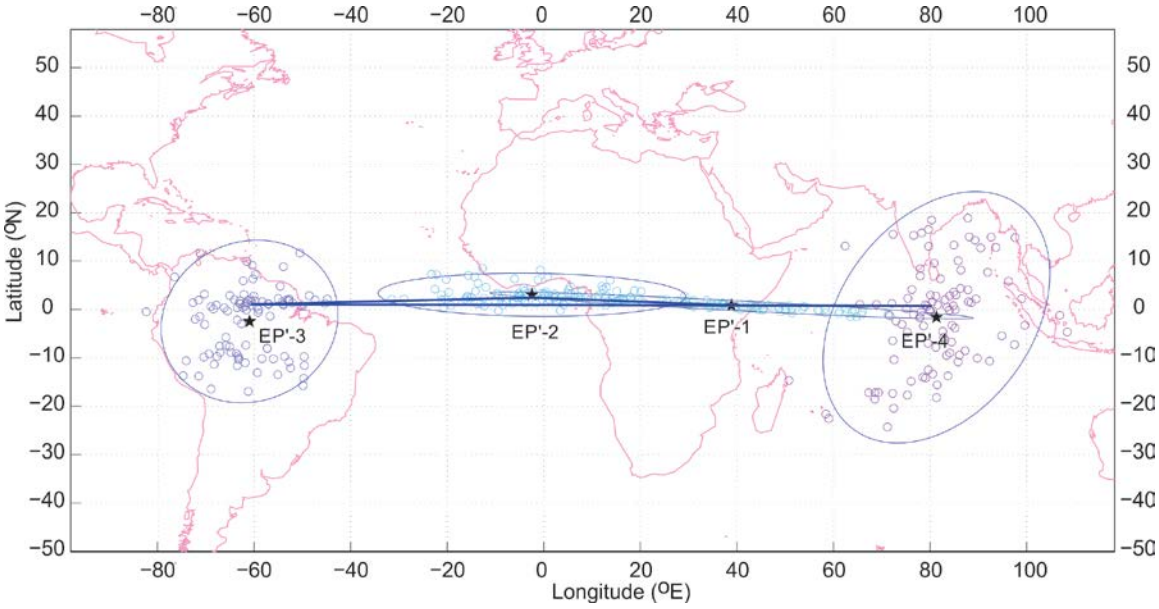

Supplementary Figure 12. Uncertainty ellipses of the bootstrapped Euler pole positions for the identified East Antarctic APWP tracks. The covariance matrices used for characterizing the ellipses are listed in Table 1. Black stars are the Fisherian means for each data set and the blue line represent the trajectory of the rotation poles.

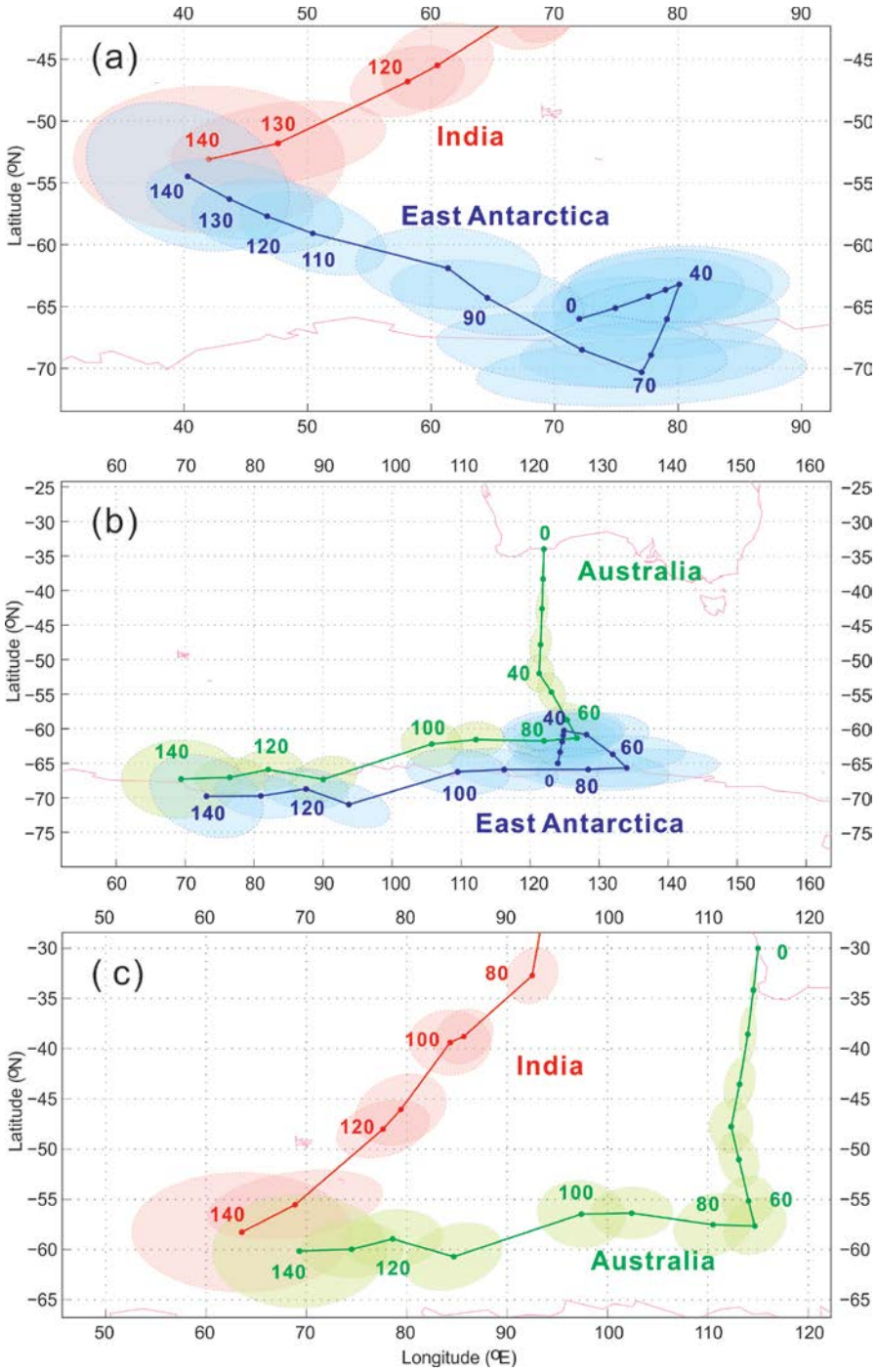

Supplementary Figure 13. To better evaluate the dispersion history among the three East Gondwana continents, we calculated the motion trajectories for different reference sites which are restored to be in proximity at the continental plate polygons at 140 Ma's reconstruction. Reconstructed positions with uncertainties are shown for (a) India (85°E, 20°N) and East Antarctica (124°E, -65°N), (b) East Antarctica (124°E, -65°N) and Australia (122°E, -34°N), and (c) Australia (115°E, -30°N) and India (96°E, 28°N).

Supplementary Movie 1. Absolute plate reconstruction of East Gondwana (India, Australia and East Antarctica) dispersion since 140 Ma (forward in time). Also shown in the movie are APWPs and corresponding A_{95}s for India (red dots and circle), Australia (blue dots and circle) and East Antarctica (green dots and circle) during each time interval.

Supplementary Movie 2. Absolute plate reconstruction of East Gondwana (India, Australia and East Antarctica) dispersion during 0 - 140 Ma (backward in time). APWPs (dots) and corresponding A_{95} s (circles) for India (red), Australia (blue) and East Antarctica (green) during each time interval are shown in the movie.

References

Besse, J., and V. Courtillot (2002), Apparent and true polar wander and the geometry of the geomagnetic field over the last 200 Myr, *Journal of Geophysical Research: Solid Earth*, *107*(B11), EPM 6–1–EPM 6–31.

Cox, A., and R. B. Hart (1986), Plate tectonics: How it works.

Fisher, N. I., T. Lewis, and M. Willcox (1981), Tests of discordancy for samples from Fisher's distribution on the sphere, *Applied Statistiss*, pp. 230–237.

Fisher, N. I., T. Lewis, and B. J. Embleton (1987), *Statistical analysis of spherical data*, Cambridge University Press.

Gordon, R. G., A. Cox, and S. O'Hare (1984), Paleomagnetic Euler poles and the apparent polar wander and absolute motion of North America since the Carboniferous, *Tectonics*, *3*(5), 499–537.

Gray, N. H., P. A. Geiser, and J. R. Geiser (1980), On the least-squares fit of small and great circles to spherically projected orientation data, *Journal of the International Association for Mathematical Geology*, *12*(3), 173–184.

Kirkwood, B. H., J.-Y. Royer, T. C. Chang, and R. G. Gordon (1999), Statistical tools for estimating and combining finite rotations and their uncertainties, *Geophysical Journal International*, *137*(2), 408–428.

Mitchell, R. N., T. M. Kilian, and D. A. Evans (2012), Supercontinent cycles and the calculation of absolute palaeolongitude in deep time, *Nature, 482*(7384), 208–211.

Scheidegger, A. E. (1965), On the statistics of the orientation of bedding planes, grain axes, and similar sedimentological data, *US Geological Survey Professional Paper, 525*, 164–167.

Smirnov, A. V., and J. A. Tarduno (2010), Co-location of eruption sites of the Siberian Traps and North Atlantic Igneous Province: Implications for the nature of hotspots and mantle plumes, *Earth and Planetary Science Letters*, *297* (3), 687–690.

Torsvik, T. H., et al. (2012), Phanerozoic polar wander, palaeogeography and dynamics, *Earth-Science Reviews*, *114* (3–4), 325–368.